Structural Engineering and Mechanics, *Vol. 57, No. 4 (2016) 733-762*
DOI: http://dx.doi.org/10.12989/sem.2016.57.4.733

Edge stresses analysis in thick composite panels subjected to axial loading using layerwise formulation

Isa Ahmadi*

Advanced Materials and Computational Mechanics Lab., Department of Mechanical Engineering, University of Zanjan, P.O. Box: 45371-38791, Zanjan, Iran

(Received October 6, 2015, Revised January 7, 2016, Accepted January 21, 2016)

Abstract. Based on a reduced displacement field, a layer-wise (LW) formulation is developed for analysis of thick shell panels which is subjected to axial tension. Employing the principle of minimum total potential energy, the local governing equations of thick panel which is subjected to axial extension are obtained. An analytical method is developed for solution of the governing equations for various edge conditions. The governing equations are solved for free and simply supported edge conditions. The interlaminar stresses in the panel are investigated by means of Hooke's law and also by means of integration of the equilibrium equations of elasticity. Dependency of the result upon the number of numerical layers in the layerwise theory (LWT) is studied. The accuracy of the numerical results is validated by comparison with the results of the finite element method and with other available results in the open literature and good agreement is seen between the results. Numerical results are then presented for the distribution of interlaminar normal and shear stresses within the symmetric and un-symmetric cross-ply thick panels with free and simply supported boundaries. The effects of the geometrical parameters such as radius to thickness and width to thickness ratio are investigated on the distribution of the interlaminar stresses in thick panels.

Keywords: thick shell panel; interlaminar stresses; layerwise theory; cross-ply laminate; free edge; simply supported edge

1. Introduction

In the composite structures, the interlaminar stresses arise in regions near the edges due to material discontinuity and mismatch in the elastic properties of adjacent layers. These stresses can lead to delamination and failure of laminated composites at loads that are much lower than the failure loads predicted by the classical lamination theories. Accurate determination of three-dimensional stress state in the boundary-layer regions of laminated plates and shells is therefore crucial in order to correctly describe the laminates behavior and to prevent their early failure. The interlaminar stress distribution in the composite laminates has been investigated by different researchers and analytical and numerical methods are used for prediction of the interlaminar stresses in composite plates and shells. The survey paper of Kant and Swaminathan (2000) reviews the appropriate papers and different methods on the interlaminar stresses in laminated composite

*Corresponding author, Assistant Professor, E-mail: i_ahmadi@znu.ac.ir

http://www.techno-press.org/?journal=sem&subpage=8 ISSN: 1225-4568 (Print), 1598-6217 (Online)

plates and shells until 2000. For completeness, however, the pertinent references on the subject are discussed here. Pipes and Pagano (1970, 1974) employed the finite difference method to generate numerical results for interlaminar stresses in symmetric balanced laminates using the reduced form of the elasticity equations. Pipe and Daniel (1971) verified that in laminated plates the free-edge effect is confined to a boundary-layer region approximately equal to the laminate thickness. Tang and Levy (1975) used the boundary-layer theory to study the interlaminar stresses in symmetric laminated composite plates in extension. Later Hsu and Herakovich (1977) studied edge effects in symmetric angle-ply composite laminates by using a perturbation technique. Wang and Choi (1982 a, b) studied the boundary-layer effects in symmetric balanced laminate by means of Lekhnistskii's stress potentials. Wang and Crossman (1977 a, b) studied the edge-effect problem of a symmetric balanced composite laminate under uniaxial extension and thermal effects by finite element method. Whitcomb *et al*. (1982) investigated the discrepancies in the results obtained by various authors and the reliability of the finite element approach. Murthy and Chamis (1989) determined interlaminar stresses in composite laminates under various loadings such as in-plane and out-of-plane shear/bending by using a three dimensional finite element method.

Cho and Kim (2000) proposed an iterative method and determined the stresses in composite laminates subjected to extension, bending, twisting and thermal loads by using the complementary virtual work and the extended Kantorovich method. Tahani and Nosier (2003) studied the free-edge stresses in general cross-ply composite laminates under extensional and thermal loadings by using the layerwise laminated plate theory (LWT). Tong *et al*. (2001), Wu (2005), Ding *et al*. (2010) studied the interlaminar stresses in composite laminates using the finite element method. Shim and Lagace (2005) present an analytical method to determine the interlaminar stresses in laminates with ply drop-offs. Wu and Chen (2010) introduced a local global higher order theory including interlaminar stress continuity for cross-ply composite and sandwich plate.

Kapoor *et al*. (2013) studied the interlaminar stresses in composite and sandwich plate using the non-uniform rational B-spline Isogeometric finite element method. They used the first order shear deformation theory to derive the governing equation.

Sarvestani and Sarvestani (2011) studied the interlaminar stress in general laminated composite plate subjected to extension and bending. Ahn and Woo (2014) studied the interlaminar stresses at free edge in laminated composite in extension and flexure using the mixed global local approach and a mixed dimensional transition element. Huang and Kim (2015) used the extended Kantorovich method to study the interlaminar stress in free edge of piezo-bonded composite laminates.

In the field of the analysis of the interlaminar stresses in composite shells and panels Franklin and Kicher (1968) used a shear deformation shell theory to analyze stresses in a laminated composite circular cylinder. Walts and Winson (1976) determined the interlaminar stresses in a laminated cylindrical shell subjected to symmetric loadings using a simplified discrete-layer shell theory. Li *et al*. (1985) obtained an analytical solution for the interlaminar stresses in a fiber-reinforced double-layer cylindrical shell. Ren (1987) presented an exact elastic solution for laminated cylindrical shells in cylindrical bending. Chaudhuri (1990) presented a semi-analytical approach for the prediction of interlaminar shear stress distribution in a thick laminated general shell. He assumed transverse inextensibility for the shell and used a layer-wise constant shear angle theory. Varadan and Bhaskar (1991) presented a 3-D elasticity solution for cross-ply simply-supported cylindrical shells subjected to a sinusoidal load. Kant and Menon (1991) used a C^0 finite element formulation and a finite difference scheme to determine interlaminar stresses in fiber-reinforced cylindrical shells under normal loads. They have used a nine-node quadrilateral shell

element with nine degrees of freedom per node. Wang and Li (1992) presented an analytical elasticity solution for interlaminar stresses in cross-ply cylindrical shells with various edge supports which subjected to a radial pressure and thermal loading. Bhaskar and Varadan (1993) used the first-order shear deformation shell theory (FSDT) to determine interlaminar stresses in laminated composite cylindrical shells under a dynamic transverse loading. They used the Navier approach and Laplace transforms technique to solve the appropriate governing equations of motion. Ramalingeswara and Ganesan (1996) compared the interlaminar stresses in cross-ply spherical shells subjected to uniform external pressure as obtained within FSDT, higher-order shear deformation shell theory with thickness stretch (HSDT7), higher order shear deformation shell theory with higher-order inplane displacement terms (HSDT9), and a three-dimensional finite element model. Later, they presented a comparative study on the interlaminar stresses in a cross-ply spherical shell subjected to a uniform external pressure using FSDT, HSDT7, HSDT9 and the 3-D finite element model (Ramalingeswara and Ganesan, 1997). Wang *et al*. (2002) derived an analytical solution based on series solution for determining the interlaminar stresses in cross-ply cylindrical shell subjected to radial pressure with simply supported ends. Kim *et al*. (2002) studied the interlaminar stresses in a shell panel with piezoelectric patch including the thermal loading using the finite element method. Faghiano *et al*. (2010) studied the calculation and recovery of the interlaminar stresses in the composite shell in the three dimensional finite element modeling of the structures. Nosier and Miri (2011) developed a layerwise formulation for analysis of the interlaminar stress in angle-ply thin cylindrical panels with free edge subjected to mechanical loading conditions. More recently Most *et al*. (2015) studied the error between the simple closed form analytical formulae and the full scale finite element analysis in prediction of the interlaminar stresses in curved laminates. Isavand *et al*. (2015) studied the dynamic response and of functionally gradient austenitic-ferritic steel composite panels under thermo-mechanical loadings. Also, recently Kar *et al*. (2015) studied nonlinear flexural response of laminated composite flat panel under hygro-thermo-mechanical loading conditions.

To the knowledge of the author, no paper in the literature seems to be devoted to development of the layerwise theory for analysis of the stresses in thick composite cylindrical panels. In this study the LWT is formulated for thick shell panels to determine the interlaminar stresses distribution in the interior and boundary-layer regions of thick shell panels under axial extension force or displacement for various edge conditions. Starting from a reduced displacement field for cross-ply shell panels under tension, for the first time a layerwise displacement formulation is developed for thick composite shell panels. The governing equation of the panel is obtained using the principle of minimum total potential energy. An analytical method is presented for solving the governing equation of the problem for various edge conditions. An integration method is introduced for obtaining the interlaminar stresses in thick panels in the LWT by integrating the equilibrium equation of elasticity. For the first time the interlaminar stresses in the panel are obtained by two methods: by means of Hooke's law (stress-strain relations) and also by means of integrating the equilibrium equation of elasticity. The numerical results of these two methods in prediction of the interlaminar stresses from the displacement field are investigated. For validation of the results, a finite element (FE) analysis is done and the results of the LWT by Hooke's law and integration method are compared by the results of the FE analysis in the prediction of the interlaminar stresses in thick panels. The interlamianr stresses at the interfaces and in the vicinity of edges of symmetric and un-symmetric panels for free and simply supported boundary conditions are studied and the results presented for thick and thin panels and compared by the results of the thick plate.

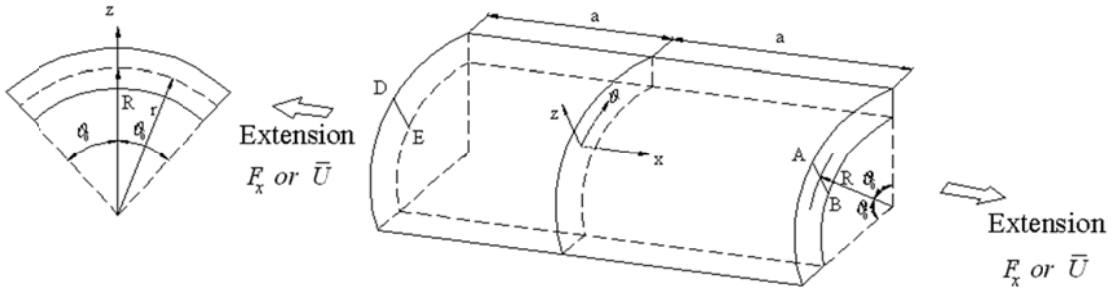

Fig. 1 Laminated circular cylindrical shell panel in extension; geometry and coordinate system

2. Theoretical formulation

A laminated thick circular cylindrical shell panel with perfectly bonded lamina and the chosen coordinate system are shown in Fig. 1.

The panel is assumed to be long and extended in the x-direction. The mean radius of the shell is R and its length is $2a$, as shown in Fig. 1. The displacement components in the x-,θ-, and r-directions of a material point initially located at the point (x,θ, r) in the k^{th} ply of the panel are denoted by $u_1^{(k)}(x,\theta, r)$, $u_2^{(k)}(x,\theta, r)$ and $u_3^{(k)}(x,\theta, r)$, respectively. The composite panel is thick and subjected to extension in axial direction. It is supposed that the fiber direction in the plies of the composite is in the x or θ direction of the panel and the composite stacking is so-called cross-ply. It is assumed that the laminated shell panel is subjected to pure extension at edges x=-a and x=+a, so that lines AB and DE has rigid displacement in x-direction without any rotation, as shown in Fig. 1. For this kind of loading, it can be shown that by assuming that the strain components are independent of the axial coordinate x, and by assuming symmetry with respect to xz plane, the displacement component in each ply of the cross-ply panel can be supposed as (Ahmadi 2005)

$$\begin{aligned} u_1^{(k)}(x,\theta,r) &= C^{(k)}x \\ u_2^{(k)}(x,\theta,r) &= v^{(k)}(\theta,r) \\ u_3^{(k)}(x,\theta,r) &= w^{(k)}(\theta,r) \end{aligned} \tag{1}$$

in which $C^{(k)}$ is the constant strain in the x-direction and $v^{(k)}(\theta, r)$ and $w^{(k)}(\theta, r)$ are unknown functions of θ and r. In order to satisfy the interfacial continuity of the displacement components in the panel, it is necessary for $C^{(k)}$ to be the same for all layers. It is clear in Fig. 1 that the r coordinate can be written as r=R+z, where R is the mean radius of the laminated shell panel and z is the thickness coordinate which is measured from the mid-plane of the panel. Thus the displacement field within the k^{th} layer of the panel may be represented as

$$\begin{aligned} u_1^{(k)}(x,\theta,z) &= Cx \\ u_2^{(k)}(x,\theta,z) &= v^{(k)}(\theta,z) \\ u_3^{(k)}(x,\theta,z) &= w^{(k)}(\theta,z) \end{aligned} \tag{2}$$

Eq. (2) represent the most general form of the displacement field within the k^{th} layer of symmetric and un-symmetric cross-ply shell panels which is subjected to pure extension. The strain components in the plies of the panel can be obtained by substituting Eq. (2) into the strain-displacement relations as

$$\begin{aligned} &\varepsilon_x^{(k)} = C = \varepsilon_0\,, \quad \varepsilon_\theta^{(k)} = \frac{1}{r} v_{,\theta}^{(k)} + \frac{1}{r} w^{(k)}, \quad \varepsilon_z^{(k)} = w_{,z}^{(k)} \\ &\gamma_{\theta z}^{(k)} = \frac{1}{r} w_{,\theta}^{(k)} - \frac{1}{r} v^{(k)} + v_{,z}^{(k)}, \quad \gamma_{xz}^{(k)} = \gamma_{x\theta}^{(k)} = 0 \end{aligned} \tag{3}$$

where in Eq. (3) and what follows, a comma followed by a coordinate indicates partial differentiation with respect to that coordinate. Relation (3) indicates that the constant C is the uniform axial strain ε_0 of the laminated shell in the x-direction. Denoting the axial displacement of the line AB by $\bar{U}$ and that of DE by $-\bar{U}$, it is then concluded that $C=\varepsilon_0=\bar{U}/a$.

2.1 Layerwise Theory of Reddy (LWT)

The displacement-based technical plate and shell theories can, in general, be classified as either equivalent single-layer (ESL) theories or layer-wise theories (see Reddy 2003). The ESL theories provide acceptable results for the global responses of thin to relatively thick laminated plates and shells but fail to give accurate results for the stresses within the boundary-layer regions of such structures. The layer-wise theories, on the other hand, are developed to provide approximately the same modeling capabilities as the full three-dimensional elasticity model. Therefore, a layer-wise theory (LWT) that possesses the capability of predicting the localized three-dimensional effects is used here to analytically study the interlaminar stresses in symmetric and un-symmetric cross-ply thick circular cylindrical shell panels.

It should to be noted that in the LWT each actual (physical) ply can be imagined to be made of p numerical (mathematical) layers with same material properties, so in the layer-wise theory, the panel is supposed to be made of N numerical layers and N+1 numerical surfaces (see Fig. 2). In the LWT, the displacements of a point in the panel are written based on the displacements of N+1 numerical surface. In order to formulate the problem by the LWT, based on the displacement field of the panel in Eq. (2), the appropriate displacement field within LWT for such panels can be written as follow

$$\begin{aligned} &u_1(x,\theta,z) = \varepsilon_0 x \\ &u_2(x,\theta,z) = V_k(\theta)\Phi_k(z) \qquad k = 1,\ldots,N+1 \\ &u_3(x,\theta,z) = W_k(\theta)\Phi_k(z) \end{aligned} \tag{4}$$

where as noted u_1, u_2 and u_3 are the displacement components of a material point located at (x,θ,z) in the un-deformed laminated shell panel in the x-, θ- and z- directions, respectively and $V_k(\theta)$ and $W_k(\theta)$ represent the displacement components of all points located on the k^{th} numerical surface within the un-deformed shell panel in θ- and z- directions, and $\Phi_k(z)$ in Eq. (4) is the global Lagrangian linear interpolation function. In the present study a repeated index indicates summation form 1 to N+1 with N being the total number of numerical layers assumed to exist within the panel. The accuracy of LWT can be improved by increasing the number of numerical (or mathematical) layers within the laminates. By increasing the number of numerical layers, as a

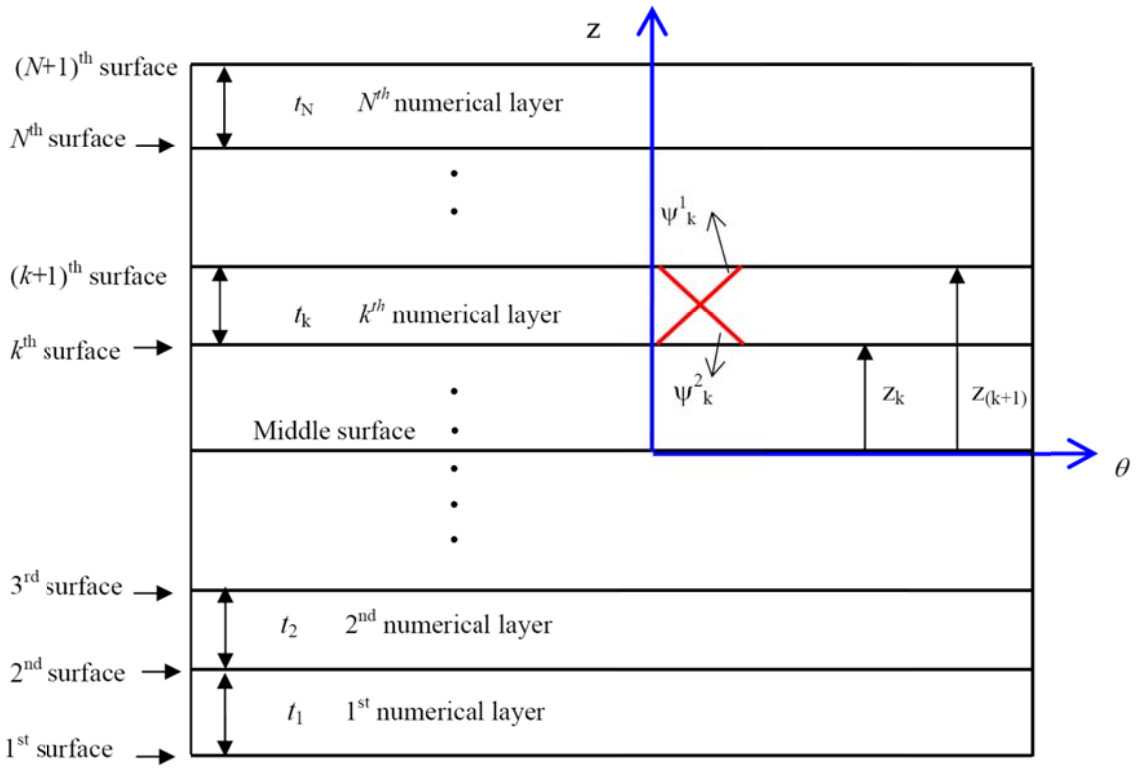

Fig. 2 Mathematical layers and local lagrangian linear interpolation function

result, the number of unknown variables in the LWT and, therefore, the number of governing equilibrium equations and the accuracy of the prediction will be increased. In the LWT, the global Lagrangian linear interpolation function $\Phi_k(z)$ is defined as

$$\Phi_k(z)=\begin{cases}0 & z \le z_{k-1}\\ \psi_{k-1}^2 & z_{k-1} \le z \le z_k\\ \psi_k^1(z) & z_k \le z \le z_{k+1}\\ 0 & z \ge z_{k+1}\end{cases} \tag{5}$$

where, $\psi^j{}_k(z)$ (j=1, 2 is superscript) are the local Lagrangian linear interpolation function within the k^{th} numerical layer of the panel (see Fig. 2). The local linear interpolation function can be written as

$$\psi_k^1(z)=\frac{1}{t_k}(z_{k+1}-z), \qquad \psi_k^2(z)=\frac{1}{t_k}(z-z_k) \tag{6}$$

2.2 LWT formulation for thick shell panel

In the analysis of thin shells in which the ratio of the thickness to the mean radius of the shell is very small i.e., $h/R<<1$, the term z/R can be neglected in comparison with 1 and the radial distance r (see Fig. 1) can be replaced by $r=R(1+z/R)\approx R$ in which R is the mean radius of the thin shell. Replacement of r by R simplifies the formulation and analysis of the problem. In the thick shells, however, the thickness of the panel, h, is comparable with the mean radius of the panel, R, and thickness to mean radius ratio of shell (h/R) cannot be neglected in comparison with 1. So in the analysis of thick shells, $1+z/R$ can not be approximated by 1 and r coordinate is usually written as $R(1+z/R)$. In order to formulate the governing equation of thick panel in the LWT, according to Eqs. (3) and (4), the strain-deformation relations for thick panel can be written as

$$\begin{aligned}
&\varepsilon_x = \varepsilon_0\ ,\quad \varepsilon_\theta = \frac{1}{R(1+z/R)}(V_k' + W_k)\Phi_k\ ,\quad \varepsilon_z = W_k\Phi_k' \\
&\gamma_{\theta z} = \frac{1}{R(1+z/R)}(W_k' - V_k)\Phi_k + V_k\Phi_k'\ ,\quad \gamma_{\theta x} = \gamma_{xz} = 0
\end{aligned} \tag{7}$$

where in Eq. (7) and the rest of the present study W_k' and V_k' indicate the ordinary differentiation of W_k and V_k with respect to θ coordinate and Φ_k' indicates the ordinary differentiation of Φ_k with respect to z coordinate.

Here, the principle of minimum total potential energy (Fung 2001) is used to obtain the equilibrium equations of the thick panel with N numerical layers within LWT. Using the principle of total potential energy, the results are $2(N+1)$ local equilibrium equations corresponding to $2(N+1)$ unknowns V_k and W_k of cross-ply panel and one global equilibrium equation corresponding to C which can be written as follow

$$\begin{aligned}
&\delta V_k: \qquad \frac{1}{R}M_\theta^k{}_{,\theta} - \tilde{Q}_\theta^k + \frac{1}{R}R_\theta^k = 0 \\
&\delta W_k: \qquad \frac{1}{R}R_\theta^k{}_{,\theta} - \tilde{N}_z^k - \frac{1}{R}M_\theta^k = 0 \\
&\delta C: \qquad F_x = \int_{\theta_0}^{\theta_0}\int_{-h/2}^{h/2} R\sigma_x(1+\frac{z}{R})dz\,d\theta
\end{aligned} \tag{8}$$

in which the generalized stress resultants for thick panel are defined as

$$\begin{aligned}
M_\theta^k &= \int_{-h/2}^{h/2}\sigma_\theta\Phi_k dz \\
R_\theta^k &= \int_{-h/2}^{h/2}\sigma_{\theta z}\Phi_k dz \\
\tilde{N}_z^k &= \int_{-h/2}^{h/2}\sigma_z\Phi_k'(1+\frac{z}{R})dz \\
\tilde{Q}_\theta^k &= \int_{-h/2}^{h/2}\sigma_{\theta z}\Phi_k'(1+\frac{z}{R})dz
\end{aligned} \tag{9}$$

Also the boundary conditions at the edges of the panel at $\theta=\pm\theta_0$ involve the specification of either V_k or M_θ^k and either W_k or R_θ^k. For example, in the free edges of the panel the boundary conditions involve specification of the generalized stress resultants $M_\theta^k=R_\theta^k=0$ which include $2(N+1)$ equations and for simply supported edges the boundary conditions involves $M_\theta^k=W^k=0$.

In order to obtain the governing equations of the panel in terms of the displacement components, the stress resultants in Eq. (9) must be expressed in terms of the displacement components. As seen in Eq. (7) , the shear strain $\gamma_{\theta x}$ and γ_{xz} vanishes in the panel and so, the stress–strain relation within the k^{th} layer of the cross-ply panel with respect to the global x-θ-z coordinate system can be written as (see, e.g., Herakovich 1998)

$$\begin{Bmatrix} \sigma_x \\ \sigma_\theta \\ \sigma_z \\ \sigma_{\theta z} \end{Bmatrix}^{(k)} = \begin{bmatrix} \overline{C}_{11} & \overline{C}_{12} & \overline{C}_{13} & 0 \\ \overline{C}_{12} & \overline{C}_{22} & \overline{C}_{23} & 0 \\ \overline{C}_{13} & \overline{C}_{23} & \overline{C}_{33} & 0 \\ 0 & 0 & 0 & \overline{C}_{44} \end{bmatrix}^{(k)} \begin{Bmatrix} \varepsilon_x \\ \varepsilon_\theta \\ \varepsilon_z \\ \gamma_{\theta z} \end{Bmatrix}^{(k)} \tag{10}$$

where in above equation $\overline{C}_{ij} = C_{ij}$ for 0°- layers and for 90°- layers $\overline{C}_{11} = C_{22}$, $\overline{C}_{22} = C_{11}$, $\overline{C}_{12} = C_{12}$, $\overline{C}_{13} = C_{23}$, $\overline{C}_{23} = C_{13}$, $\overline{C}_{33} = C_{33}$, and $\overline{C}_{44} = C_{55}$ with C_{ij}'s being the three-dimensional stiffness of an orthotropic lamina. Using the stress-strain relation in Eq. (10) and the strain-displacement relation in Eq. (7), the generalized stress resultants of thick panel can be obtained in terms of the displacement components as

$$\begin{aligned} M_\theta^k &= B_{12}^k \varepsilon_0 + \frac{1}{R}\tilde{\tilde{D}}_{22}^{kj} V_j' + (\frac{1}{R}\tilde{\tilde{D}}_{22}^{kj} + B_{23}^{kj}) W_j \\ R_\theta^k &= (B_{44}^{kj} - \frac{1}{R}\tilde{\tilde{D}}_{44}^{kj}) V_j + \frac{1}{R}\tilde{\tilde{D}}_{44}^{kj} W_j' \\ \tilde{N}_z^k &= \tilde{A}_{13}^k \varepsilon_0 + \frac{1}{R} B_{23}^{jk} V_j' + (\frac{1}{R} B_{23}^{jk} + \tilde{A}_{33}^{kj}) W_j \\ \tilde{Q}_\theta^k &= (\tilde{A}_{44}^{kj} - \frac{1}{R} B_{44}^{jk}) V_j + \frac{1}{R} B_{44}^{jk} W_j' \end{aligned} \tag{11}$$

in which the laminate rigidities in Eq. (11) are defined as follow

$$\begin{aligned} (\tilde{A}_{pq}^k, \tilde{A}_{pq}^{kj}) &= \sum_{i=1}^{N} \int_{z_i}^{z_{i+1}} \overline{C}_{pq}^{(i)} (\Phi_k', \Phi_k' \Phi_j') (1 + \frac{z}{R}) dz , \\ (B_{pq}^k, B_{pq}^{kj}) &= \sum_{i=1}^{N} \int_{z_i}^{z_{i+1}} \overline{C}_{pq}^{(i)} (\Phi_k, \Phi_k \Phi_j') dz \\ \tilde{\tilde{D}}_{pq}^{kj} &= \sum_{i=1}^{N} \int_{z_i}^{z_{i+1}} \overline{C}_{pq}^{(i)} (\Phi_k \Phi_j) (1 + \frac{z}{R})^{-1} dz , \end{aligned} \tag{12}$$

The integrations in Eq. (12) are carried out and the final expressions for the rigidities for convenience are presented in Appendix A.

By substituting Eq. (11) into Eqs. (8a) and (8b), the local equilibrium equations of the panel are expressed in terms of V_j and W_j as

$$\begin{aligned} \delta V_k : \quad & \frac{1}{R^2}\tilde{\tilde{D}}_{22}^{kj} V_j'' + (\frac{1}{R} B_{44}^{kj} + \frac{1}{R} B_{44}^{jk} - \frac{1}{R^2}\tilde{\tilde{D}}_{44}^{kj} - \tilde{A}_{44}^{kj}) V_j \\ & + \frac{1}{R}(\frac{1}{R}\tilde{\tilde{D}}_{22}^{kj} + \frac{1}{R}\tilde{\tilde{D}}_{44}^{kj} + B_{23}^{kj} - B_{44}^{jk}) W_j' = 0 \end{aligned} \tag{13a}$$

$$\begin{aligned}\delta W_k : \quad & -\frac{1}{R}\left(\frac{1}{R}\tilde{\tilde{D}}_{22}^{kj}+\frac{1}{R}\tilde{\tilde{D}}_{44}^{kj}+B_{23}^{jk}-B_{44}^{kj}\right)V_j'+\frac{1}{R^2}\tilde{\tilde{D}}_{44}^{kj}W_j'' \\ & -\left(\frac{1}{R^2}\tilde{\tilde{D}}_{22}^{kj}+\frac{1}{R}B_{23}^{kj}+\frac{1}{R}B_{23}^{jk}+\tilde{A}_{33}^{kj}\right)W_j=\left(\tilde{A}_{13}^{k}+\frac{1}{R}B_{12}^{k}\right)\varepsilon_0\end{aligned} \tag{13b}$$

and by substituting stress-strain relation into Eq. (8c), the global equilibrium equation is expressed as

$$F_x=\int_{-\theta_0}^{\theta_0}R\left[\tilde{A}_{11}\varepsilon_0+\frac{1}{R}B_{12}^{j}(V_j'+W_j)+\tilde{A}_{13}^{j}W_j\right]d\theta \tag{14}$$

where the axial rigidity $\tilde{A}_{11}$ of the panel is defined as

$$\tilde{A}_{11}=\sum_{i=1}^{N}\int_{z_i}^{z}\bar{C}_{11}^{(i)}\left(1+\frac{z}{R}\right)dz=\sum_{i=1}^{N}\bar{C}_{11}^{(i)}(t_i)\left(1+\frac{z_{i+1}+z_i}{2R}\right) \tag{15}$$

In general Eqs. (13a), (13b) and (14) involve $2N$+3 differential equations which are the local and global equilibrium equations of the panel.

3. Solution of the equations

The equilibrium equations of the panel in Eqs. (13) and (14) can be solved analytically by defining the state space variable. For solving of the equations, the new state variables are defined as

$$\begin{aligned}&\{X_1\}=\{V\},\quad \{X_2\}=\{V'\},\\ &\{X_3\}=\{W\},\quad \{X_4\}=\{W'\},\end{aligned} \tag{16}$$

in which

$$\begin{aligned}\{V\}^T&=\{V_1,V_{2,},\ldots,V_{N+1}\}\\ \{W\}^T&=\{W_1,W_{2,},\ldots,W_{N+1}\}\end{aligned} \tag{17}$$

and $\{X\}$ is defined as;

$$\{X\}=\{\{X_1\}^T,\{X_2\}^T,\{X_3\}^T,\{X_3\}^T\}^T \tag{18}$$

Substitution of Eq. (16) into Eq. (13) and Eq. (14) yield the local equilibrium equations in Eq. (13) in the standard form as

$$\{\dot{X}\}=[A]\{X\}+\{F\}\varepsilon_0 \tag{19}$$

and the global equilibrium equation in Eq. (14) can be written as

$$F_x=\int_{-\theta_0}^{\theta_0}\{\bar{M}\}\{X\}d\theta+(2R\theta_0\tilde{A}_{11})\varepsilon_0 \tag{20}$$

in which $[A]$ and $\{F\}$ is defined in Appendix B and $\{\bar{M}\}$ is defined as

$$\{\bar{M}\}=\left\{\{0\}^T,\{B_{12}\}^T,\{B_{12}\}^T+R\{\tilde{A}_{13}\}^T,\{0\}^T\right\} \tag{21}$$

in which $\{0\}^T$ is the zero vector with (N+1) rows and $\{B_{12}\}$ and $\{\tilde{A}_{13}\}$ is define in appendix A.

3.1 Loading conditions

For a panel which is subjected to axial extension, two kinds of extension load can be considered as shown in Fig. 1.

1. Extension displacement as $\pm\bar{U}$ at $x=\pm a$ which causes axial strain as $\varepsilon_0=\bar{U}/a$.

2. Tension force as $\pm F_x$ at $x=\pm a$ in which the axial strain must be obtained by simultaneously solution of Eqs. (19) and (20).

If the axial strain $\varepsilon_0=\bar{U}/a$ is supposed to be a known loading parameter during the solution i. e. $\bar{U}$ is determined in loading, then the unknowns include $2N$+2 functions V_k and W_k which can be obtained by solving Eq. (19) and then the applied force F_x can be obtained by Eq. (20).

On the other hand, if axial force F_x is supposed to be the known extension force in the loading, then the axial strain ε_0 is unknown, and ($2N$+1) unknowns of the problem should be obtained by simultaneously solution of Eqs. (19) and (20). In this kind of loading some researchers such as Tahani and Nosier (2003) used the equivalent single layer (ESL) to obtain the axial stress ε_0 and used this strain as the known solution parameter in the LWT. Although the ESL theories have adequate accuracy in prediction of the global response of composite laminates, but this approach reduces the accuracy of the predicted results especially for thick panels. In this study, full layerwise method formulation is used for solution of the problem in the case of axial extension displacement and axial tension Force.

3.1.1 Panel subjected to axial extension $\bar{U}$

If the axial extension displacement $\bar{U}$ of the panel is known, then the axial strain ε_0 is known as $\varepsilon_0=\bar{U}/a$. In this case, Eq. (19) can be solved independently. For this aim the new variable $\{S\}$ is defined as

$$\{X\}=[U]\{S\} \tag{22}$$

in which $[U]$ is the modal matrix (i.e., matrix of eigenvectors) of $[A]$ so that

$$[A][U]=[U][\Lambda] \tag{23}$$

and $\lambda_1, \lambda_2,..., \lambda_{4(N+1)}$ are the eigenvalues of the matrix $[A]$ in which

$$\mathbf{[\Lambda]}=diag(\lambda_1,\lambda_2,...,\lambda_{4(N+1)}) \tag{24}$$

Substitution of Eq. (22) into Eq. (19) and multiplying by $[U]^{-1}$ from the left yields

$$\{\dot{S}\}=[\Lambda]\{S\}+[U]^{-1}\{F\}\varepsilon_0 \tag{25}$$

It is clear that $[\Lambda]$ is a diagonal matrix and so, Eq. (25) can be solved analytically. By solving Eq. (25) and substituting the subsequent result in Eq. (22), $\{X\}$ can be obtained as

$$\{X\}=[U][\exp(\lambda\theta)]\{K\}-[A]^{-1}\{F\}\varepsilon_0 \tag{26}$$

which

$$[\exp(\lambda\theta)] = diag\,(\exp(\lambda_1\theta), \exp(\lambda_2\theta), ..., \exp(\lambda_{4(N+1)}\theta)) \tag{27}$$

and $\{K\}$ being $4(N+1)$ unknown integration constants and must be obtained by imposing the boundary conditions at $\theta=\pm\theta_0$.

3.1.2 Panel subjected to axial force F_x

In this kind of loading the panel is subjected to an axial force F_x instead of axial extension displacement $\bar{U}$, and so the axial strain ε_0 is unknown parameter during the solution. In this case, Eqs. (19) and (20) should be solved simultaneously. For this purpose, Eq. (26) is substituted in Eq. (20) and the result is written as

$$F_x = \{\bar{M}\}[U][\Lambda]^{-1}([\exp(\lambda\theta_0)] - [\exp(-\lambda\theta_0)])\{K\} + 2\theta_0(R\tilde{A}_{11} - \{\bar{M}\}[A]^{-1}\{F\}\,)\varepsilon_0 \tag{28}$$

Now the axial strain ε_0 can be obtained using Eq. (28) as

$$\varepsilon_0 = \{\bar{\beta}\}\{K\} + \frac{F_x}{\bar{E}} \tag{29}$$

in which $\bar{E}$ and $\{\bar{\beta}\}$ are defined as

$$\bar{E} = 2\theta_0(R\tilde{A}_{11} - \{\bar{M}\}[A]^{-1}\{F\}) \tag{30}$$

$$\{\bar{\beta}\} = -\frac{1}{\bar{E}}\{\bar{M}\}[U][\Lambda]^{-1}([\exp(\lambda\theta_0)] - [\exp(-\lambda\theta_0)]) \tag{31}$$

Now, the general solution of $\{X\}$ can be obtained by substituting Eq. (29) into Eq. (26) as

$$\{X\} = ([U][\exp(\lambda\theta)] - [A]^{-1}\{F\}\ \{\bar{\beta}\})\{K\} - (\frac{1}{\bar{E}}[A]^{-1}\{F\})F_x \tag{32}$$

Same as Eq. (26), Eq. (32) contains $4(N+1)$ unknown constant $\{K\}$ and can be obtained by imposing the boundary conditions at $\theta=\pm\theta_0$.

3.2 Boundary conditions

The boundary conditions of the panel include determining either V_k or M_θ^k and either W_k or R_θ^k at the edges of the panel at $\theta=\theta_0$ and $\theta=-\theta_0$. The boundary conditions at the free edges of the panel include determining M_θ^k and R_θ^k as

$$\begin{matrix} M_\theta^k = 0 \\ R_\theta^k = 0 \end{matrix} \quad \text{at } \theta = \pm\theta_0 \tag{33}$$

and the simply supported edge of the panel can be considered by imposing the following conditions at the edges of the panel.

$$\begin{matrix} M_\theta^k = 0 \\ W^k = 0 \end{matrix} \quad \text{at } \theta = \pm\theta_0 \tag{34}$$

The boundary conditions of the panel in Eq. (33) or Eq. (34) include 4(N+1) equations, and the integration constants $\{K\}$ in Eq. (26) or Eq. (32) can be obtained by imposing the boundary conditions to the equations.

3.3 Evaluation of the stresses

After solving of the governing equations, the stresses in the panel can be obtained by the Hooke's law (stress-strain relation). The interlaminar strains which are obtained from the LWT are not continuous at the numerical surfaces. So the values of interlaminar stresses at the numerical surfaces predicted by Hooke's law are not continuous. On the other hand, the alternative method for prediction of interlaminar stresses in the panel is integration of the equilibrium equations of the panel. The equilibrium equations of the theory of elasticity in θ and r direction in the cylindrical co-ordinate can be written as

$$\begin{aligned} &\frac{\partial(r^2\ \sigma_{\theta r})}{\partial r}+r\frac{\partial \sigma_\theta}{\partial \theta}=0 \\ &\frac{\partial(r\ \sigma_r)}{\partial r}-\sigma_\theta+\frac{\partial \sigma_{\theta r}}{\partial \theta}=0 \end{aligned} \tag{35}$$

The interlaminar stresses, $\sigma_{\theta r}=\sigma_{\theta z}$ and $\sigma_r=\sigma_z$ can be obtained by integration of Eq. (35). In the LWT, the interlaminar shear stress $\sigma_{\theta z}$ and normal stress σ_z at the n^{th} numerical surface i.e., $z=z_n$, $1 \le n \le N+1$ can be obtained by integration of Eq. (35). For this aim, by substituting σ_θ from Eq. (10) and Eq. (7) in the first equation of Eq. (35) and integrating from z_1 to z_n, the interlaminar shear stress $\sigma_{\theta r}$ can be obtained as

$$\begin{aligned} \sigma_{\theta r}(z_n)&=\frac{-1}{r^2}\int_{z_1}^{z_n}[\bar{C}_{22}(V_k''+W_k')\Phi_k+\bar{C}_{23}rW_k'\Phi_k']dz \\ &=\frac{-1}{r_n^2}\sum_{k=1}^{n}(B_{22}^k(V_k''+W_k'))+R\tilde{B}_{23}^kW_k') \end{aligned} \tag{36}$$

Also by substituting from Eq. (10) and Eq. (7) for σ_θ and $\sigma_{\theta r}$ in the second equation of Eq. (35), the interlaminar normal stress σ_r can be obtained as

$$\begin{aligned} \sigma_r(z_n)&=\frac{1}{r_n}\int_{z_1}^{z_n}[\bar{C}_{22}(\frac{V_k'+W_k}{r})\Phi_k+\bar{C}_{23}W_k\Phi_k'-\bar{C}_{44}((\frac{W_k'-V_k}{r})\Phi_k+V_k\Phi_k')]dz \\ &=\frac{1}{r_n}\sum_{k=1}^{n}(\frac{1}{R}\tilde{\tilde{B}}_{22}^k(V_k'+W_k)+A_{23}^kW_k-\frac{1}{R}\tilde{\tilde{B}}_{44}^k(W_k'-V_k)-A_{44}^kV_k+\bar{A}_{12}\varepsilon_0 \end{aligned} \tag{37}$$

in which the coefficients matrix is defined as below and are obtained in appendix A.

$$\begin{aligned} \tilde{A}_{pq}^k&=\int_{z_1}^{z_n}\bar{C}_{pq}\Phi_k'(1+z/R)dz=\sum_{i=1}^{n-1}\int_{z_i}^{z_{i+1}}\bar{C}_{pq}^{(i)}\Phi_k'(1+z/R)dz \\ B_{pq}^k&=\int_{z_1}^{z_n}\bar{C}_{pq}\Phi_k dz=\sum_{i=1}^{n-1}\int_{z_i}^{z_{i+1}}\bar{C}_{pq}^{(i)}\Phi_k dz \\ \tilde{\tilde{B}}_{pq}^k&=\int_{z_1}^{z_n}\bar{C}_{pq}\Phi_k(1+z/R)^{-1}dz=\sum_{i=1}^{n-1}\int_{z_i}^{z_{i+1}}\bar{C}_{pq}^{(i)}\Phi_k(1+z/R)^{-1}dz \end{aligned} \tag{38}$$

Table 1 Mechanical properties of T300/5052 Graphite/Epoxy lamina (Herakovich 1998)

E_1 (GPa)	E_2=E_3 (GPa)	G_{12}=G_{13} (GPa)	G_{23} (GPa)	ν_{12}=ν_{13}	ν_{23}
132	10.8	5.65	3.35	0.24	0.59

4. Numerical results and discussions

In order to investigate the interlaminar stresses in the thick composite panel, the numerical results for several thick shell panels which are subjected to axial extension force are presented. The mean radius, thickness and width of the panel are shown by R, h and $2b$, respectively. Laminated Graphite/Epoxy panel with symmetric and un-symmetric cross-ply layer stacking are investigated in the analysis. The typical elastic properties of the Graphite/Epoxy ply are given in Table (1). It is supposed that the thickness of all plies of the Graphite/Epoxy in the panel is the same and equals to h_k and the physical layers of the laminated panel are fully banded at the interfaces.

4.1 Convergence study

As said before, in the LWT each physical layer is assumed to be made of several imagined layer with the same fiber directions with the actual layers. These imagined layers are called the numerical (mathematical) layers. The number of subdivision of each physical layer can be different from layer to layer. In this study, all physical layers are divided into same mathematical layer. If the number of subdivisions of each physical layers be same and equal to p, then the total numerical layers of the panel will be equal to N=$p\tilde{N}$ in which $\tilde{N}$ is the number of physical layers in the laminate and the total number of numerical surfaces will be equal to N+1. The accuracy of the LWT depends on the number of numerical layers in the panel and in order to increase the accuracy of the numerical results, the number of subdivision of each layer p, and the number of total numerical layers N must be increased.

In what follows, first the convergence of the stresses in the panel with free edge and simply supported edge with the increasing of the numerical layers is studied and then several numerical examples are presented for cross-ply thick shell panels subjected to extension. In this study the dimensionless stresses are defined as σ^*=$\sigma/\bar{\sigma}$ in which $\bar{\sigma}$ is the average axial stress in the panel due to the extension force F_x and defined as $\bar{\sigma}$=$F_x/(2bh)$ in which $2b$=$2R\theta_0$ is the average width of the panel (the width on the mean radius) of the panel. The convergence of the interlaminar normal stress, σ_z at the edge θ=θ_0, of the panel with free edge and simply supported edge is shown in Fig. 3 and Fig. 4, respectively. In these figures the interlaminar stress σ_z is obtained by integrating the equilibrium equations in (38). In the figures, h_k is the thickness of the physical layers. The numerical and physical surfaces and layers of the panel are numbered from the inner surface of the panel to the outer surface. According to the coordinate, z/h_k=0 indicates the middle surface of the panel. For the laminates with 4 physical layers, z/h_k=-1 indicates the interface of first layer (interior layer) and second layer and z/h_k=1 shows the interface of third and fourth layer and z/h_k=-2 and z/h_k=2 indicate the inner and outer surface of the panel, respectively.

Fig. 3 shows the value of the interlaminar normal stress σ_z exactly at the free edge of the thick panel with R/h=5 and $2b/h$=3 in $[0°/90°]_s$, $[90°/0°]_s$ and [0°/90°/0°/90°] lamination stacking for various number of subdivision p. At the free edge, it is seen that in the 0°/0° and 90°/90° interface

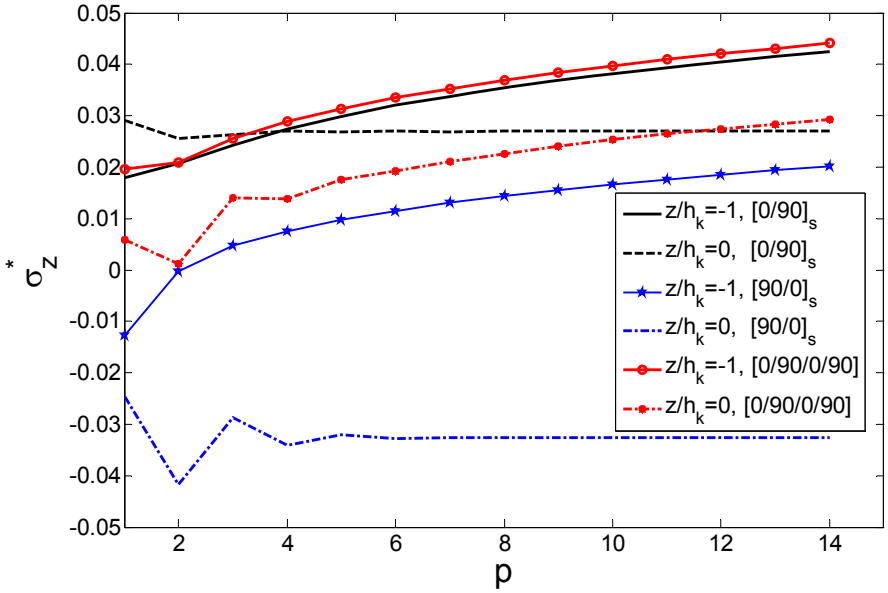

Fig. 3 Convergence study of interlaminar normal stress σ_z at the free edge in thick panel versus p, R/h=5, 2b/h=3

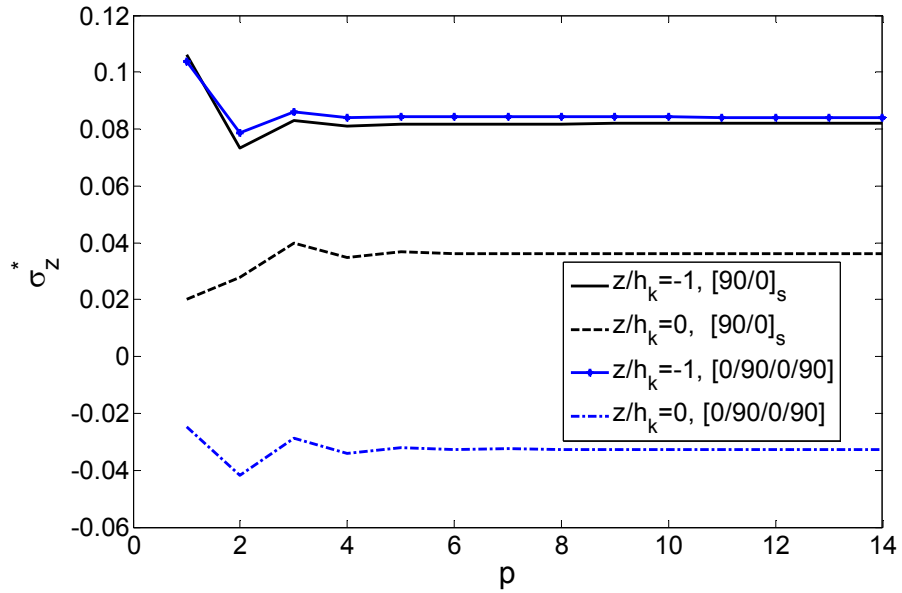

Fig. 4 Convergence study of interlaminar normal stress σ_z at simply supported edge in thick panel versus p, R/h=5, 2b/h=3

which the two adjacent layer have the same fiber orientation, the σ_z is converged with increasing of the numerical subdivision p and for p>5 the value of σ_z remains constant. At the 0°/90° and 90°/0° interfaces, the value of σ_z is increased monotonically by increasing the number of

subdivisions. So, it seems to be no stress singularity in the free edge at 0°/0° and 90°/90° interfaces which adjacent layers have same material properties. In the free edge at the interface of the layers which have different elastic properties i.e., 0°/90° and 90°/0° interfaces, it is seen that the value of σ_z grows monotonically as p increases which suggest that stress singularity may exist at 0°/90° and 90°/0° interfaces, but such a conclusion can not be proven by the approximate theories.

The convergence study of panel with simply supported edges, of the interlaminar normal stress at the edge ($\theta=\theta_0$) in $[90°/0°]_s$ and [0°/90°/0°/90°] panel is studied in Fig. 4. It is seen that at the simply supported edges, the interlaminar normal stress σ_z converged to a constant value for 0°/0°, 0°/90° and 90°/0° interfaces by increasing of the numerical subdivision p and monotonically increasing is not seen in simply supported edges. In the analysis of the interlaminar stresses in order to have a good accuracy the number of subdivision of physical layer is chosen to be p=10 for free edge and simply supported edge.

4.2 Investigation of interlaminar stresses

The distribution of the interlaminar stresses in $[0°/90°]_s$, $[90°/0°]_s$ and [0°/90°/0°/90°] Graphite/Epoxy thick panels subjected to axial extension force as F_x is studied in this section. In order to obtain the results with adequate accuracy, the number of subdivision of each physical layer is taken p=10 and so, the total number of numerical surfaces in the panel is 41 surfaces. As mentioned before, after solving the governing equations of the system, the interlaminar stresses can be obtained by two methods: 1- By using the Hooke's law in Eq. (10), 2- By integrating the equilibrium equations in Eq. (37) and Eq. (38) as an alternative method. In the LWT with C^0 Lagrangian interpolation function, the continuity of the interlaminar strains ε_z and $\gamma_{\theta z}$ is not guaranteed at the interface of two adjacent numerical layers. For example, the interlaminar strains at the k^{th} numerical surface ($z=z_k$) can be obtained by the upper numerical layer of that surface i.e., displacements of $(k+1)^{th}$ and k^{th} surface, also the interlaminar strains at the k^{th} surface can be obtained by the numerical layer that located under the k^{th} layer i.e., $(k\text{-}1)^{th}$ and k^{th} surfaces. The strain at k^{th} surface which is obtained from the upper layer is denoted by ε^{k+}, and the strain which is obtained from the under layer is denoted by ε^{k-}. So, in prediction of the interlaminar stresses at k^{th} surface by the Hooke's law, two values can be obtained for the interlaminar stress σ_z and $\sigma_{\theta z}$. The interlaminar stresses at k^{th} surface which is obtained by the elastic properties of the upper numerical layer, and the strains obtained by the upper layer, ε^{k+} are shown by σ^{k+}. The interlaminar stresses at k^{th} surface can also be obtained by the elastic properties of the $(k\text{-}1)^{th}$ numerical layer, and the strains obtained by the under numerical layer of that surface, ε^{k-} and are denoted by σ^{k-}. So in the predictions of Hooke's law, the interlaminar stresses are not continuous at the interface of the layers i.e., σ^{k-} may not equal to σ^{k+}. In this study the Hooke's law stress is obtained as the average of two value as $\sigma^k=0.5(\sigma^{k-}+\sigma^{k+})$. On the other hand, the integration method which is introduced in Eq. (37) and Eq. (38) gives a unique value for the interlaminar normal and shear stresses at the interfaces. In what follows, the distribution of the interlaminar stresses in Graphite/Epoxy thick panel with free edges and simply supported edges are studied and the effects of radius to thickness R/h and width to thickness $2b/h$ on the interlaminiar stresses are investigated.

4.2.1 Verification of the results

The Finite Element method (FEM) is used for verification of the results of the presented method. The results of the finite element model are obtained by a 3D model in the commercial

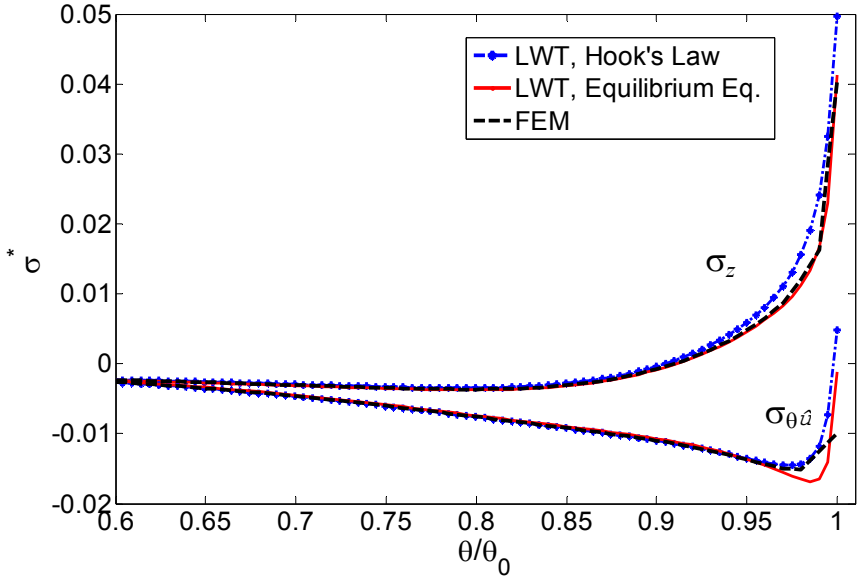

Fig. 5 Comparison of the predictions of LWT and FEM for interlaminar normal and shear stress at $z=h_k$ in the $[0/90]_s$ panel, (R/h=5, $2b/h$=4)

finite element code Ansys using solid46 element. In the model the thickness, width and length of the panel are divided into 48, 200 and 5 element respectively and the 0° and 90° plies are modeled as two separate materials with different material properties. The model is subjected to axial extension force. In order to compare the results of the FEM and LWT the distribution of the interlaminar stresses through some paths in the circumferential and thickness direction of $[0/90]_s$ thick panel (R/h=5) is investigated in Fig. 5 to Fig. 7. In order to study the distribution of the interlaminar stress at the interface of the adjacent layer with different fiber orientation, Fig. 5 compares the results of the LWT and the FEM at the interface of third and forth physical layer ($z=h_k$) of $[0/90]_s$ panel. The prediction of LWT by Hooke's law, the prediction of LWT by integration of equilibrium equations, and the prediction of the FEM are shown in Fig. 5. It is seen that the prediction of the LWT by integration method and the prediction of FEM for interlaminar normal stress σ_z are in close agreement. Also it is seen that the prediction of the FEM and the LWT for $\sigma_{\theta z}$ is in close agreement unless just near the free edge. For more investigation on the prediction of LWT and FEM, the distribution of the interlaminar normal stress σ_z and shear stress $\sigma_{\theta z}$ through the thickness of the panel are shown in Fig. 6 and Fig. 7. Fig. 6 shows the normal stress through the thickness of the panel at the free edge ($\theta=\theta_0$) and in the vicinity of the edge at $\theta=0.99\theta_0$, $\theta=0.98\theta_0$, $\theta=0.96\theta_0$, $\theta=0.94\theta_0$, and at $\theta=0.8\theta_0$ which is predicted by the LWT and FEM. Solid lines show the prediction of the LWT with equilibrium equation and dashed lines show the prediction of FEM. In Fig. 6 very good agreement is seen between the predictions of FEM and prediction of the LWT by integration method for σ_z unless slight difference is seen in the interface of the layers with different fiber orientation at $z=\pm z_k$ near the free edge. The distribution of the interlaminar shear stress $\sigma_{\theta z}$ through the thickness of the panel is shown in Fig. 7. It is clear that at the free edge, the shear stress $\sigma_{\theta z}$ must be vanished, but it is seen that at the interface of the adjacent layers with different material properties ($z=\pm z_k$), the shear stress $\sigma_{\theta z}$ which is predicted by

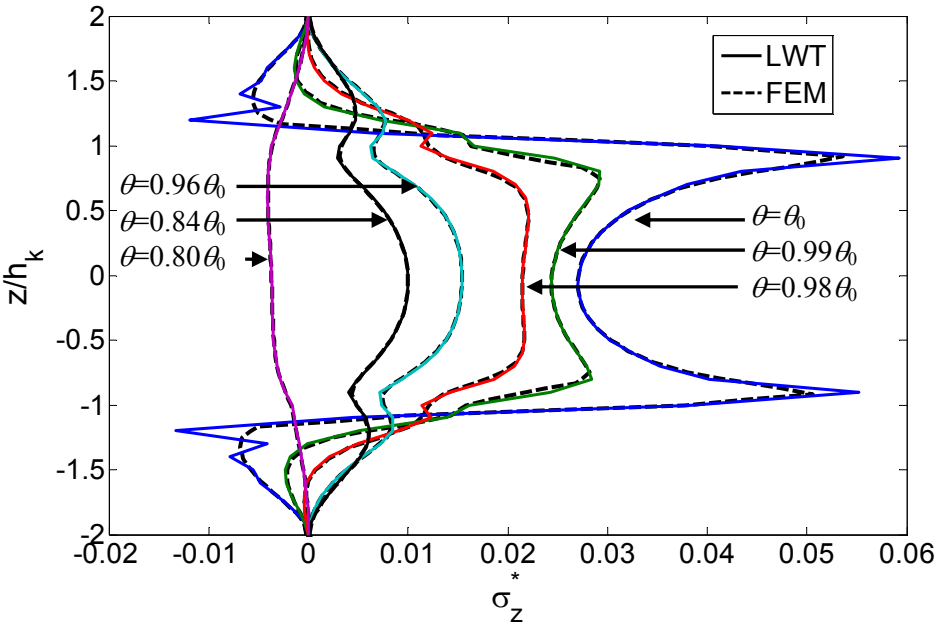

Fig. 6 Comparison of the predictions of LWT and FEM for interlaminar normal stress σ_z in the $[0/90]_s$ panel, (Solid lines: LWT, Dashed lines: FEM, R/h=5, $2b/h$=4)

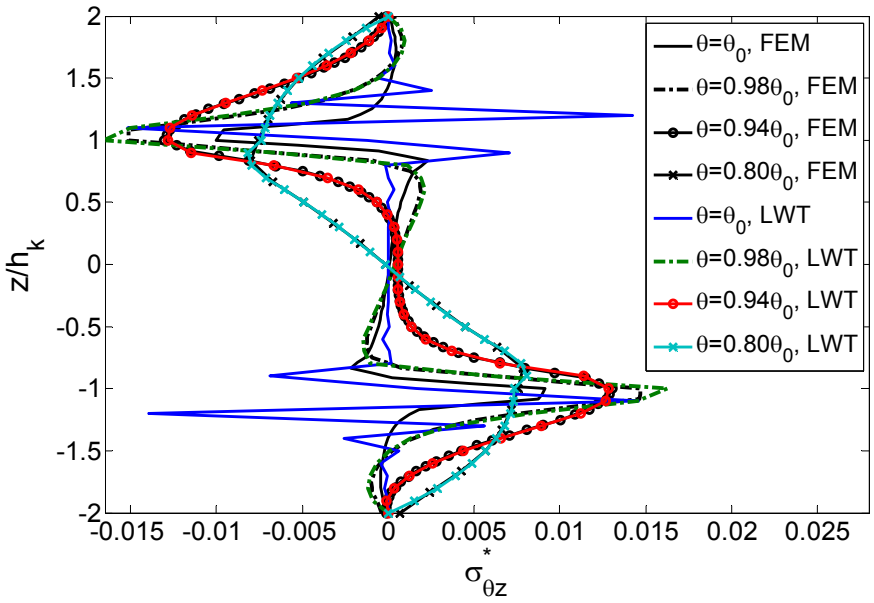

Fig. 7 Comparison of the predictions of LWT and FEM for interlaminar shear stress $\sigma_{\theta z}$ in the $[0/90]_s$ panel, (R/h=5, $2b/h$=4)

the LWT and FEM is not zero. At the free edge, $\sigma_{\theta z}$ which is predicted by the LWT has sharp disturbance near $z=\pm h_k$. It is seen that the interlaminar shear stress decreases far from the free

edges (θ=0.8θ_0) and increases rapidly in the vicinity of the free edge. It is seen that except at the free edge (θ=θ_0) that the predictions of the methods are not in agreements, at θ=0.98θ_0, θ=0.94θ_0 and θ=0.8θ_0 the prediction of the LWT and FEM are in close agreement.

In Fig. 6 and Fig. 7, it is seen that at z/h_k=±2 which is the free outer and inner surface of the panel, the interlaminar normal and shear stresses vanished. The interlaminar normal stress near the points (θ=θ_0, z/h_k=±1) increased rapidly and has a peak. As seen in Fig. 3, the value of σ_z at this point increased monotonically by increasing the number of numerical layer in the LWT. From the predicted results which are shown in Fig. 5 to Fig. 7, it is concluded that the prediction of presented LW formulation and FEM for interlaminar stresses are in close agreement and the accuracy of the LW Formulation for prediction of interlaminar stresses in thick panel is examined.

4.2.2 Free edge conditions

The distribution of the interlaminar stresses in the thick panels with free edges is studied in this section. The distribution of the interlaminar stresses in the panel with lamination sequence as $[90°/0°]_s$ and the same geometry as previous example (R/h=5 and 2b/h=4) are shown in Fig. 8 and Fig. 9. The distribution of the interlaminar normal and shear stress in $[90°/0°]_s$ panel at z=-h_k and z=0 are shown in Fig. 8. As said before, the prediction of Hooke's law is not continuous at the interfaces and two values are presented for predictions of Hooke's law: prediction by upper layer (σ_z^+) and lower layer (σ_z^-). This figure shows the predictions of integral method (equilibrium equations) and also the predictions of Hooke's law by upper numerical layer i.e., σ_z^+ and under numerical layer i.e., σ_z^-. As seen, there is considerable difference between σ_z^+, σ_z^- and prediction by the integral method. It must be noted that in this panel b=2h and so it can be concluded from Fig. 8 that the thickness of the boundary layer is approximately about the thickness of the panel and the interlaminar stresses almost vanished for θ<0.5θ_0.

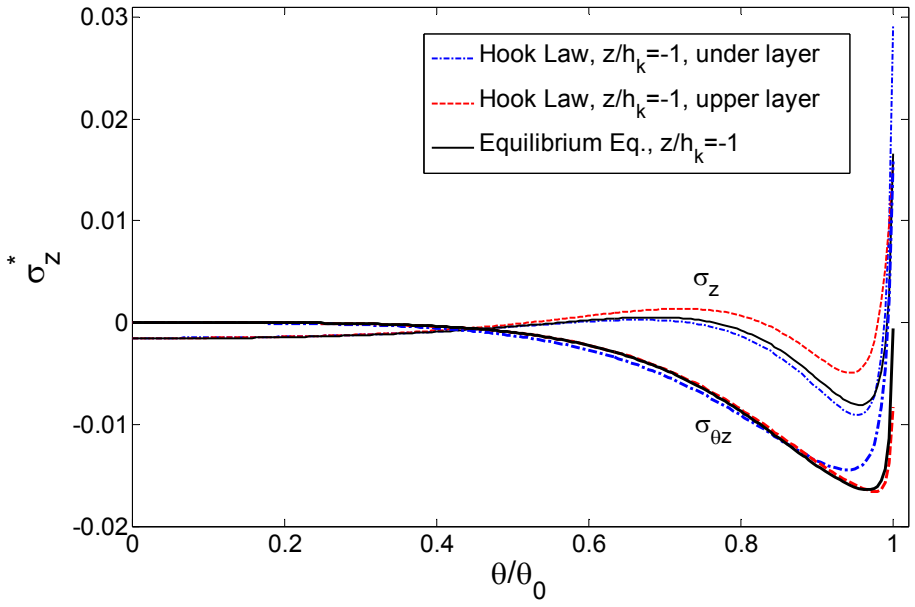

Fig. 8 Distribution of σ_z and $\sigma_{\theta z}$ in the $[90°/0]_s$ panel at z/h_k=-1, (R/h=5, 2b/h=4)

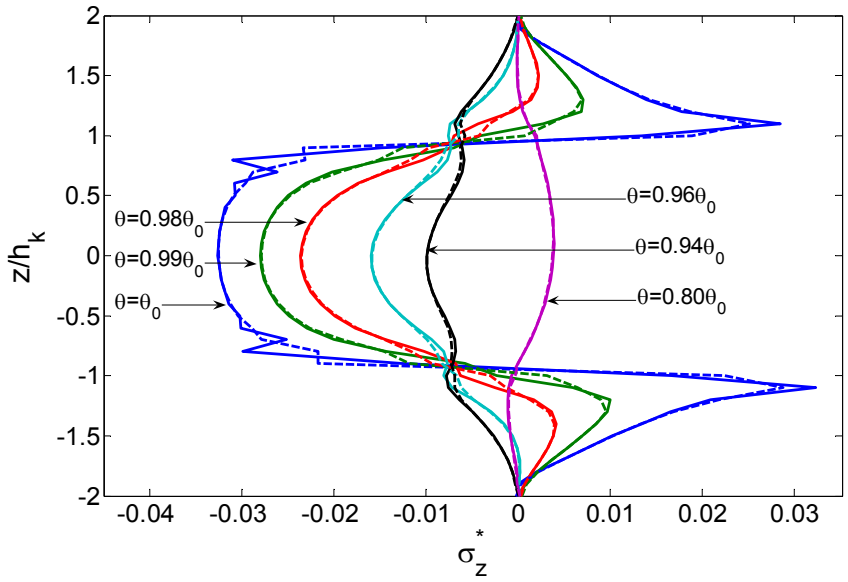

Fig. 9 Distribution of σ_z through the thickness of the $[90°/0]_s$ panel, (Solid lines: equilibrium equation, Dashed lines: Hook's law) (R/h=5, $2b/h$=4)

Physically, for example when [90°/0°/0°/90°] panel is subjected to extension in the axial direction as ε_0, 0° laminas and 90° laminas tend to contract in the transverse direction (θ direction) as $\nu_{12}\varepsilon_0$ and $\nu_{21}\varepsilon_0$, respectively. It is clear that ν_{12} is very bigger than ν_{21} and so $\nu_{12}\varepsilon_0 > \nu_{21}\varepsilon_0$. So in the extension, the contract of 90° layers is less than the contract of 0° layers. The lamina in the laminate are banded in the interfaces and so this mismatch in the transverse contraction of the layers induces shear stress $\sigma_{\theta z}$ in the interface of layers near the edges. This shear stress is so that it tries to match the contraction of 0° and 90° layers. For example in the [90°/0°/0°/90°] panel, 0° layers insert shear stress in the interface to the inner and outer 90° layers in order to increase their contraction and vice versa, 90° layers insert shear stress to 0° layers in the interfaces in the opposite direction to decrease the contraction of 0° layers. It is clear that shear stress in the surfaces on 90° layers is toward the free edge and on the 0° layers is in the opposite side. So in the right half of the panel which θ>0°, the induced shear stress $\sigma_{\theta z}$ in the layer interface on 0° layers is toward the edge in order to decrease the contraction of 0° layers and vice versa on 90° layers this shear stress is in opposite direction in order to increase the contraction of 90° layers to match with the contraction of 0° layers. So in [90°/0°/0°/90°] panel in the right half of the panel which θ>0°, at the interface of first and second layer at z/h_k=-1, i.e., 90°/0° interface the shear stress $\sigma_{\theta z}$ is negative and at the interface of third and forth layers at z/h_k=1, i.e., 0°/90° interface the shear stress is positive. It is seen in Fig. 8 that for θ>0° the model predicts negative $\sigma_{\theta z}$ at z/h_k=-1. Same interpretation could be presenter for other laminate sequence. The existence of the interlaminar normal stress near the edge can be explained by considering the free body diagram of a piece of the lamina in the laminate near the edges. For example σ_z on the interface must be self equilibrium and so σ_z is positive in free edge and negative in some other zone near so that its integration on the interface must vanish for free edge.

For more study on the distribution of the interlaminar normal stress in the vicinity of the free

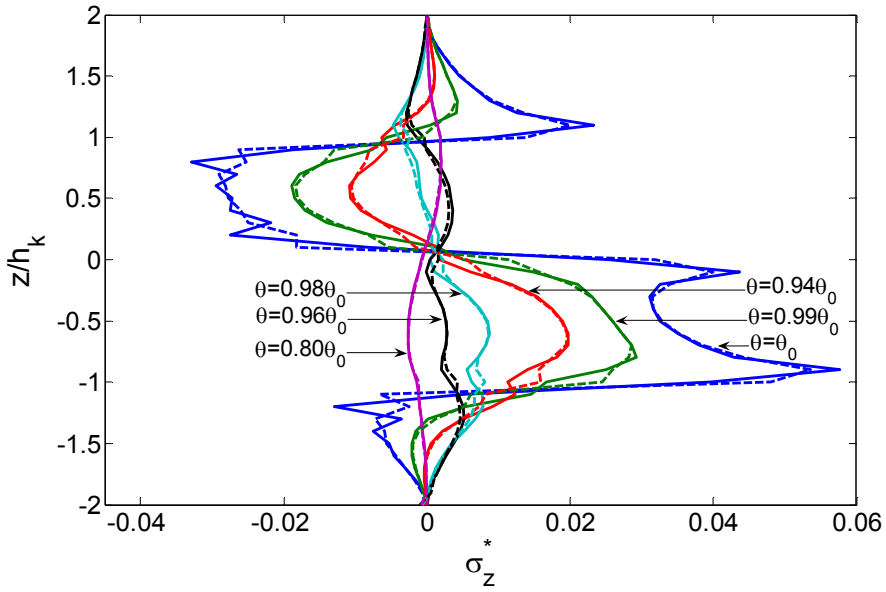

Fig. 10 Distribution of σ_z through the thickness of the [0/90°/0/90°] panel, (Solid lines: Equilibrium Equation, Dashed lines: Hook's law) (R/h=5, $2b/h$=4)

edge of the composite panel, the distribution of the interlaminar normal stress σ_z through the thickness of symmetric $[90°/0°]_s$ and un-symmetric [0°/90°/0°/90°] thick panel are shown in Fig. 10. These Figure shows the average value of prediction of Hooke's law, i.e., $\sigma_z=0.5(\sigma_z^+ + \sigma_z^-)$ (dashed lines) and the prediction of the LWT by equilibrium equation (solid lines). It is seen that except at the interfaces of layers with different fiber orientation, the prediction of the Hooke's law (average value) is in very close agreement with predictions of equilibrium equations. A slight difference is seen near the free edge near $z=\pm h_k$. It is observed that the interlaminar normal stress in the 90° plies of the $[90°/0°]_s$ is positive and sharply changed at the interfaces to the negative value at 0° plies. It is seen that the pattern of the distribution of the interlaminar normal stress is different in $[90°/0°]_s$ and [0°/90°/0°/90°] panel.

4.2.3 Parametric study (R/h and 2b/h effect)

The effect of the radius to thickness ratio, R/h, on the distribution of the interlaminar stress in $[90°/0°]_s$ panel with $2b/h$=4 is studied in Fig. 11 and Fig. 12. Fig. 11 shows the distribution of the σ_z on z/h_k=-1 of the $[90°/0°]_s$ panel for various radius to thickness ratio (R/h) ratio. This figure also contains the prediction of the $[90°/0°]_s$ plate with the same geometry by (Tahani and Nosier 2003). It is seen that by increasing the R/h ratio the distribution of the interlaminar stresses at the panel tends to the distribution for the stresses in the plate and for R/h=50 the distribution of σ_z in panel and plate in coincides. It can be seen that for large R/h (thin panel), far from the free edge, σ_z vanishes at the interior zone of the panel and for small R/h ratio, σ_z is compressive at $z=-h_k$. The effect of R/h ratio on the distribution of $\sigma_{\theta z}$ in $[90°/0°]_s$ panel with $2b/h$=4 are studied in Fig. 12. It is seen that R/h ratio has slight effect on the distribution of the interlaminar shear stress in the vicinity of the free edge. For R/h=50, the distribution of the $\sigma_{\theta z}$ at the panel is same as the plate. It can be concluded that for large R/h the interlaminar stresses at panel and plate is very close and for

R/h>20 plate theories can be used for prediction of the interlaminar stresses in the panel with adequate accuracy. In Fig. 12, it is seen that the thickness of the boundary layer is about the thickness of the panel.

The distribution of the interlaminar normal stress σ_z and shear stress $\sigma_{\theta z}$ in $[90°/0°]_s$ panel with R/h=5 and for various width to thickness ratio $2b/h$ are shown in Fig. 13 and Fig. 14, respectively.

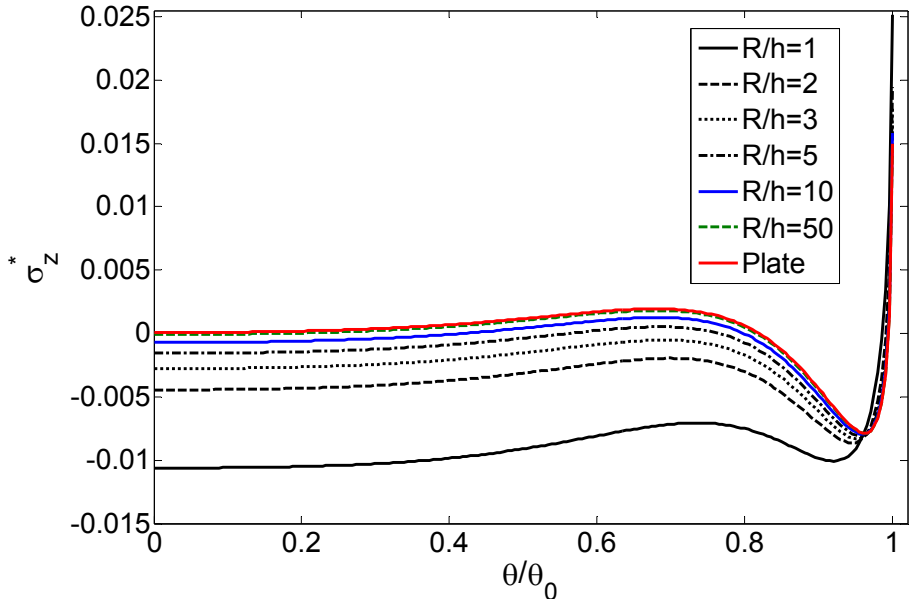

Fig. 11 Effect of R/h ratio on the distribution of σ_z at z/h_k=-1 of $[90°/0]_s$ panel, ($2b/h$=4)

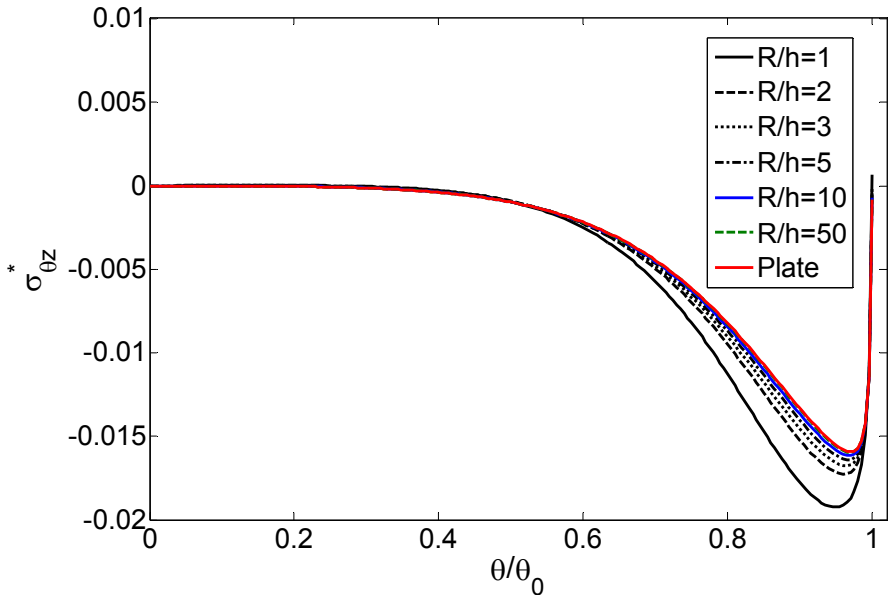

Fig. 12 The effect of R/h ratio on the distribution of $\sigma_{\theta z}$ at z/h_k=-1 of $[90°/0]_s$, ($2b/h$=4)

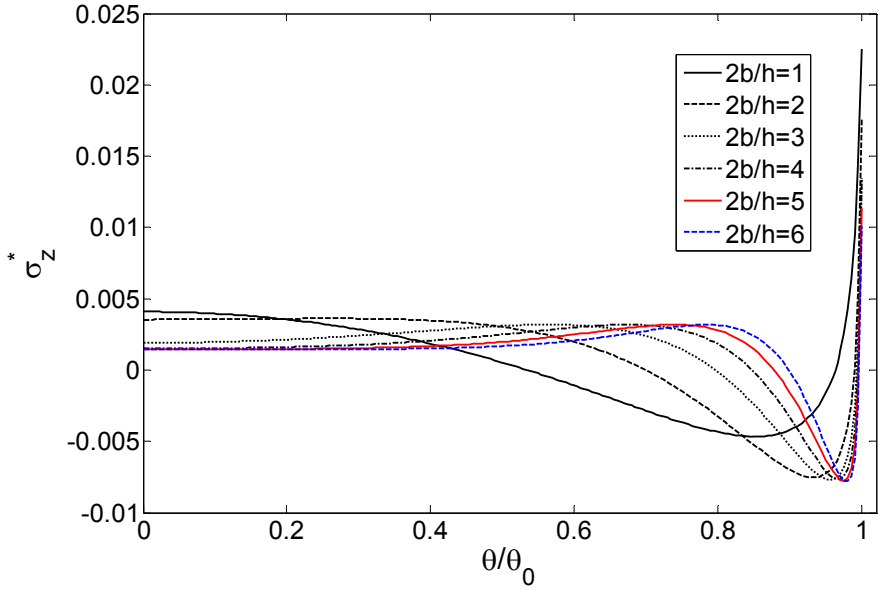

Fig. 13 Effect of $2b/h$ ratio on the distribution of σ_z at z/h_k=1 of $[90°/0]_s$, (R/h=5)

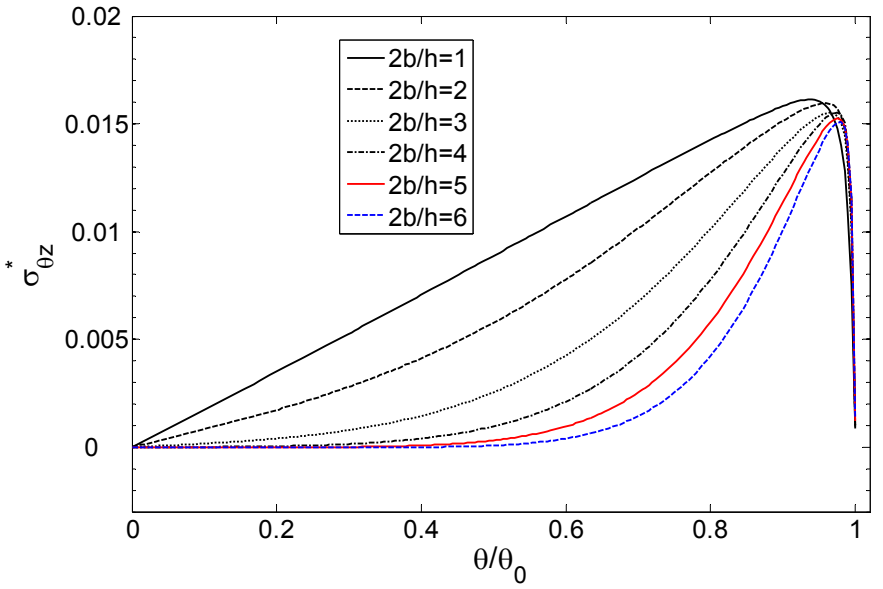

Fig. 14 Effect of $2b/h$ ratio on the distribution of $\sigma_{\theta z}$ at z/h_k=1of $[90°/0]_s$, (R/h=5)

It is seen that by decreasing the width to thickness ratio of the panel, the distribution of the σ_z and especially $\sigma_{\theta z}$ developed to the interior zone of the panel. For large $2b/h$ the interlaminar stresses is confined in a small layer near the edge.

In other to study the predictions of LWT in prediction of the inplane stresses, the distribution of σ_θ through the thickness of the $[90°/0°]_s$ panel in the vicinity of the free edge is shown in Fig. 15.

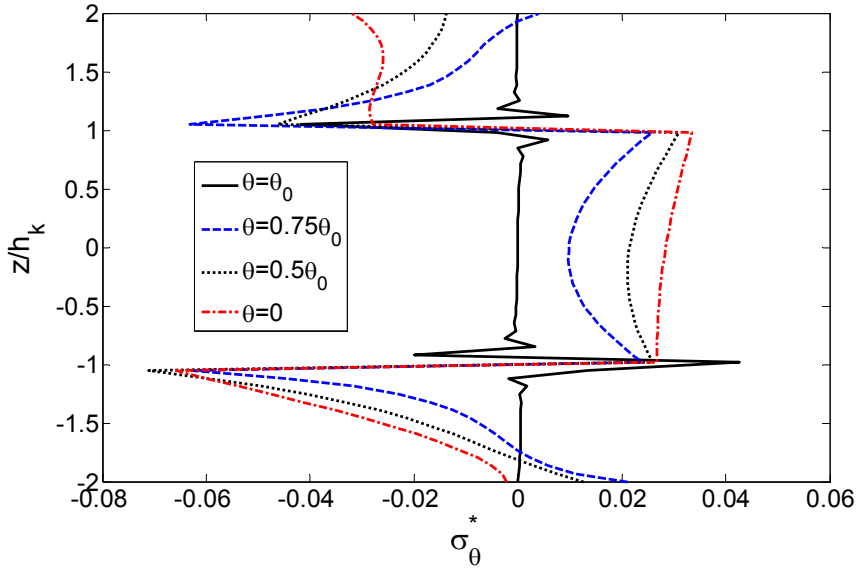

Fig. 15 Distribution of the in-plane stress σ_θ through the thickness of $[90°/0]_s$ panel, (R/h=2, $2b/h$=2)

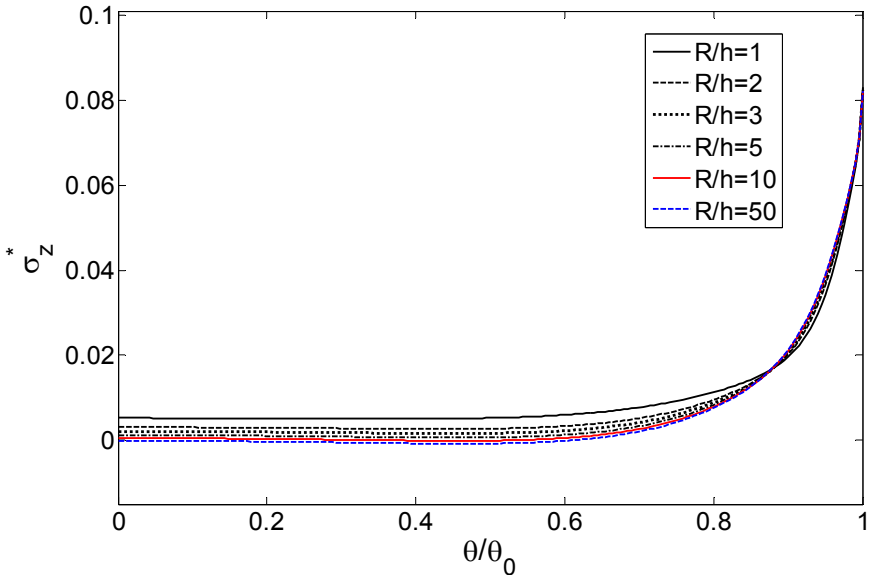

Fig. 16 Distribution of σ_z at z/h_k=1 of $[90°/0]_s$ panel with simply supported B.C. ($2b/h$=4)

It is seen that the σ_θ is tensile in 0° layers and is compressive in 90°layers. It is seen that σ_θ vanished at the free edge unless near the interface of 0° and 90° layers.

4.2.4 Simply supported boundary conditions

The distribution of the interlaminar normal and shear stress in the panel which is subjected to simply supported boundary conditions at $\theta=\pm\theta_0$ are investigated in this section. The distribution of

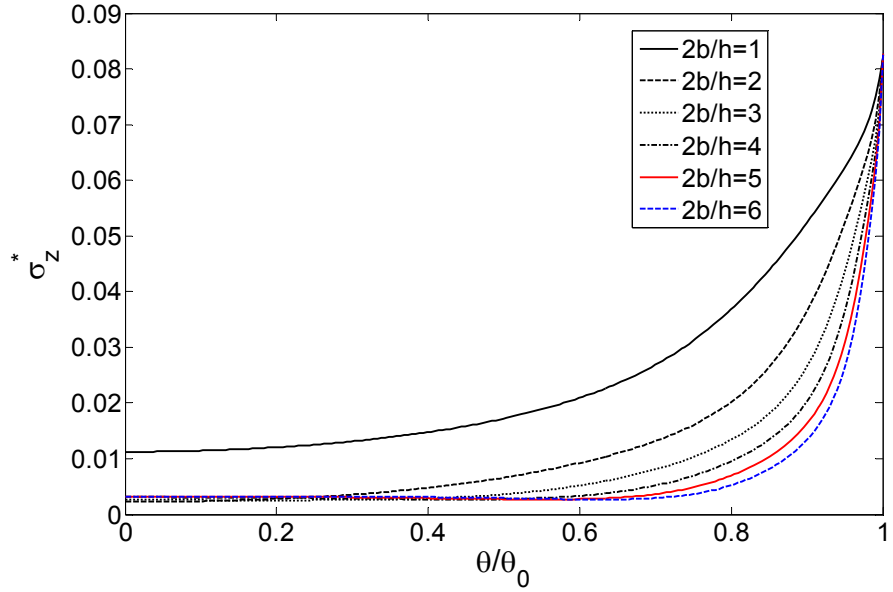

Fig. 17 Distribution of σ_z at z/h_k=1 of $[90°/0]_s$ panel with simply supported B.C. (R/h=2)

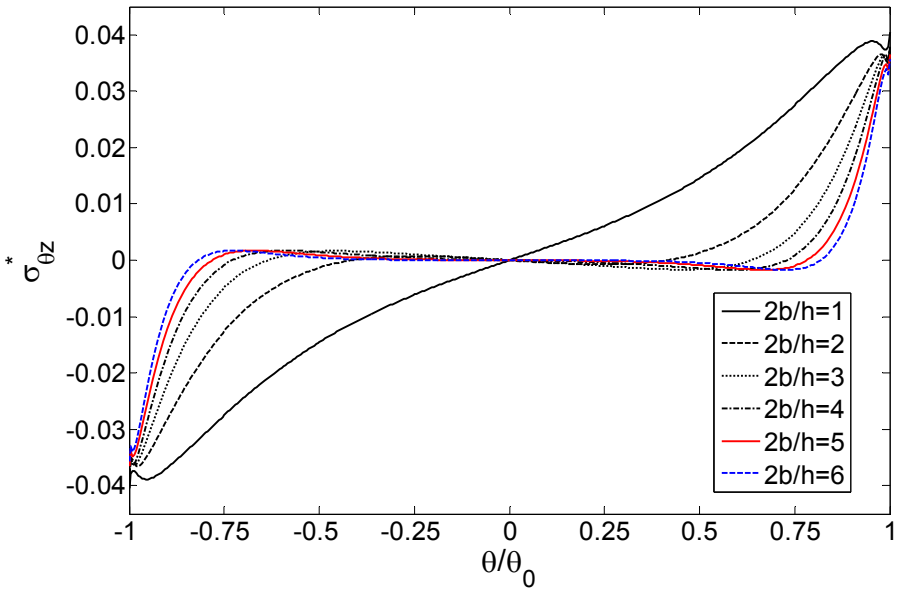

Fig. 18 Distribution of $\sigma_{\theta z}$ at z/h_k=1 of $[90°/0]_s$ panel with simply supported B.C. (R/h=2)

σ_z at z/h_k=1 of thick $[90°/0°]_s$ panel with simply supported B.C with $2b/h$=4 and for various R/h ratio are shown in Fig. 16. As seen in the Figure, in the panel with simply boundary conditions, R/h has slight effect on the distribution of the interlaminar normal stress in the interior region and the value of σ_z at the edge ($\theta=\theta_0$) does not depend on the R/h.

The distribution of the interlaminar normal and shear stress at z/h_k=1 of $[90°/0°]_s$ panel with

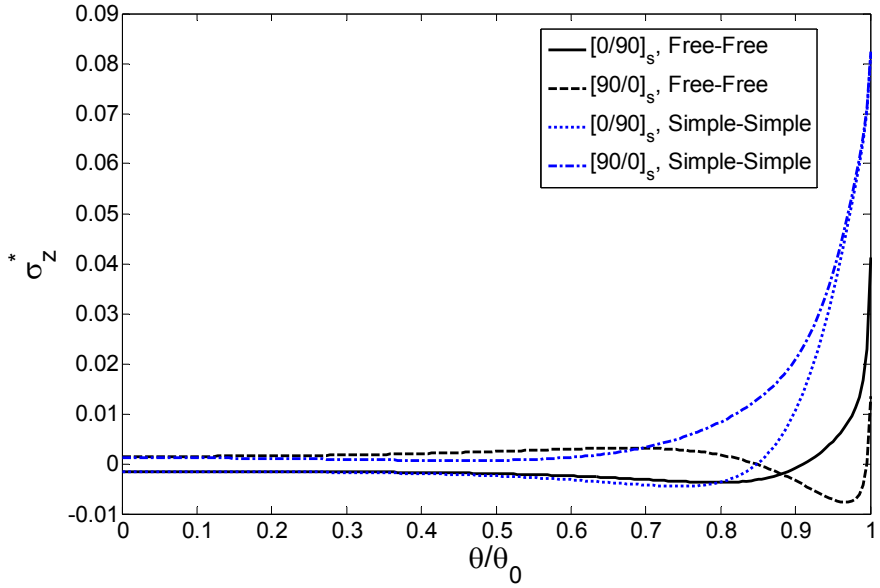

Fig. 19 Distribution of σ_z at z/h_k=1 of thick panels for free and simple B.C. (R/h=5, 2b/h=4)

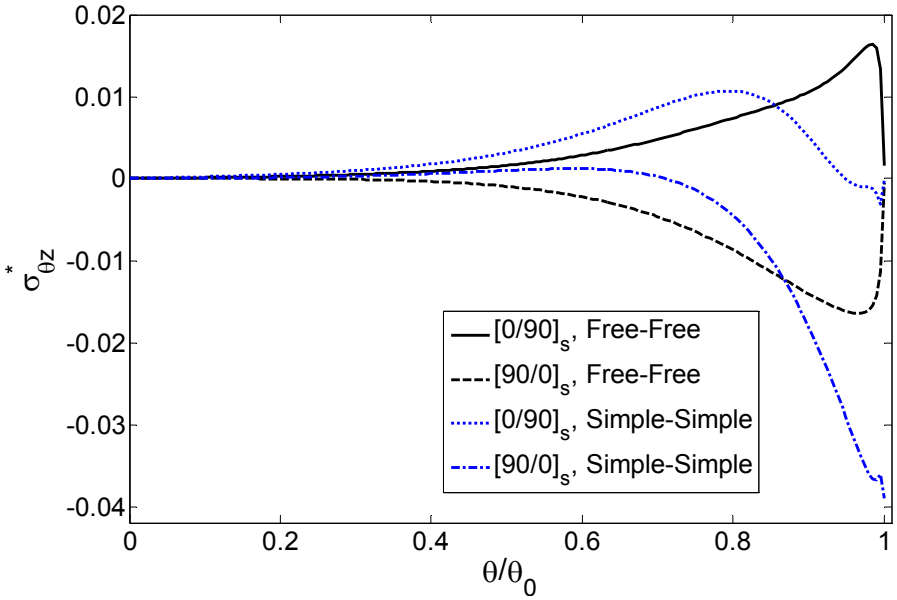

Fig. 20 Distribution of σ_z at z/h_k=-1 of thick panels for free and simple B.C. (R/h=5, 2b/h=4)

simply supported B.C for R/h=2 and various 2b/h are shown in Fig. 17 and Fig. 18, respectively. It is seen that for simply supported edges, the interlaminar stresses exactly at the simply supported edge do not depend on the R/h and 2b/h ratio.

The distribution of the interlaminar stresses in the panel with free edge and simply supported edge for $[0°/90°]_s$ and $[90°/0°]_s$ panel with R/h=5 and 2b/h=4 are shown and compared in Fig. 19

and Fig. 20. Fig. 19 shows the distribution of the interlaminar normal stress σ_z at $z=h_k$ and Fig. 20 shows the shear stress $\sigma_{\theta z}$ at $z=-h_k$ of the panels with free edges and with simply supported edges. It is seen that σ_z at simply supported edge is bigger than the free edge. The pattern of the distribution of the stresses is different in simply supported and free edge.

5. Conclusions

A displacement based LWT formulation is derived for analysis of thick laminated panel subjected to axial extension force or displacement. The governing equations and appropriate boundary conditions for cross-ply thick panel in the LWT are derived based on the principle of the minimum total potential energy. An analytical method is presented for solution of the governing equation of the panel for extension force and extension displacement and the governing equations are solved for free and for simply supported boundaries at the edges of the panel. The interlaminar stresses at the interfaces and in the vicinity of free and simply supported edges of panels are studied. An integration method is introduced for obtaining the interlaminar stresses and the interlaminar stresses in the panel are obtained by two methods: by employing the Hooke's law (stress-strain relations) and by integrating the elasticity equilibrium equation of the panel as an alternative method. The effect of the number of numerical layer on the convergence of the interlaminar stresses is investigated. The prediction of the Hooke's law and prediction of Equilibrium equations are presented and compared in the numerical results by the results of the FE analysis and the results of thick plate. In the numerical results, the interlaminar stresses in the vicinity of the edges of the laminated symmetric and un-symmetric cross-ply composite panel are studied and the effects of R/h and $2b/h$ on the distribution of the stresses are investigated. It is seen that if the Hooke's law is used for evaluation of the interlaminar stresses the average value which is obtained from the upper and lower numerical layer has sufficient accuracy. It is concluded that for $R/h>20$, the plate theory can be used for prediction of the interlaminar stresses in the panel with adequate accuracy.

References

Ahmadi, I. (2005), "Analysis of interlaminar stresses in thin composite shells", MSc. Thesis, Sharif University of Technology, Tehran, Iran.

Ahn, J.S. and Woo, K.S. (2014), "Interlaminar stress distribution of laminated composites using the mixed-dimensional transition element", *J. Compos. Mater.*, **48**(1), 3-20.

Bheskar, K. and Varadan, T.K. (1993), "Interlaminar stresses in composite cylindrical shells under transient loads", *J. Sound Vib.*, **168**(3), 469-477.

Chaudhuri, R.A. (1990), "On the prediction of interlaminar stresses in a thick laminated general shell", *Int. J. Solid. Struct.*, **26**(5-6), 499-510.

Cho, M. and Kim, H.S. (2000), "Iterative free-edge stress analysis of composite laminates under extension, bending, twisting and thermal loadings", *Int. J. Solid. Struct.*, **37**(3), 435-459.

Ding, S., Tong, J.W., Shen, M. and Huo, Y. (2010), "Three-Dimensional elastic-plastic analysis of the interlaminar stresses for the AS4/PEEK composite laminate with a circular hole", *Mech. Adv. Mater. Struct.*, **17**(6), 406-418.

Fagiano, C., Abdalla, M.M. and Gürdal, Z. (2010), "Interlaminar stress recovery of multilayer composite shell structures for three-dimensional finite elements", *Finite Elem. Anal. Des.*, **46**(12), 1122-1130.

Franklin, H.G. and Kicher, T.P. (1968), "Stresses in laminated composite cylinders", *AIAA J.*, **6**(11), 2208-2209.
Fung, Y.C. and Tong, P. (2001), *Classical and Computational Solid Mechanics*, World Scientific, New Jersey.
Herakovich, C.T. (1998), *Mechanics of Fibrous Composite*, John Wiley & Sons, New York.
Hsu, P.W, and Herakovich, C.T. (1977), "Edge effects in angle-ply composite laminate", *J. Compos. Mater.*, **11**(4), 422-428.
Huang, B. and Kim, H.S. (2015), "Interlaminar stress analysis of piezo-bonded composite laminates using the extended Kantorovich method", *Int. J. Mech. Sci.*, **90**(1), 16-24.
Isavand, S., Bodaghi, M., Shakeri M. and Mohandesi J.A. (2015), "Dynamic response of functionally gradient austenitic-ferritic steel composite panels under thermo-mechanical loadings", *Steel Compos. Struct.*, **18**(1), 1-28.
Kant, T. and Menon, M.P. (1991), "Estimation of Interlaminar Stresses in Fiber Reinforced Composite Cylindrical Shells", *Comput. Struct.*, **38**(2), 131-147.
Kant, T. and Swaminathan, K. (2000), "Estimation of transverse/interlaminar stresses in laminated composites-a selective review and survey of current developments", *Compos. Struct.*, **49**(1), 65-75.
Kapoor, H., Kapania, R.K. and Soni, S.R. (2013), "Interlaminar stress calculation in composite and sandwich plates in NURBS isogeometric finite element analysis", *Compos. Struct.*, **106**(1), 537-548.
Kar, V.R., Mahapatra, T.R. and Subrata, K.P. (2015), "Nonlinear flexural analysis of laminated Composite flat Panel under hygro-thermo-mechanical loading", *Steel Compos. Struct.*, **19**(4), 1011-1033.
Kim, H.S., Zhou, X. and Chattopadhyay, A. (2002), "Interlaminar stress analysis of shell structures with piezoelectric patch including thermal loading", *AIAA J.*, **40**(12), 2517-2525.
Li, S., Wang, R. and Luo, Z. (1985), "An analytic solution for interlaminar stresses in a fiber reinforced double-layer cylindrical shell", *Acta Mech.*, **1** (2), 159-170.
Miri, A.K. and Nosier, A. (2011), "Interlaminar stresses in antisymmetric angle-ply cylindrical shell panels", *Compos. Struct.*, **93**(2), 419-429.
Most, J., Stegmair, D. and Petry, D. (2015), "Error estimation between simple, closed-form analytical formulae and full-scale FEM for interlaminar stress prediction in curved laminates", *Compos. Struct.*, **131**(1), 72-81.
Murthy, P.L.N. and Chamis, C.C. (1989), "Free-edge delamination: laminate width and loading conditions effects", *J. Comp. Technol. Res.*, **11**(1), 15-22.
Pipes, R.B. and Daniel, I.M. (1971), "Moire analysis of the interlaminar shear edge effect in laminated composites", *J. Compos. Mater.*, **5**(2), 255-259.
Pipes, R.B. and Pagano, N.J. (1974), "Interlaminar stresses in composite laminates-an approximate elasticity solution", *J. Appl. Mech.*, **41**(3), 668-672.
Pipes, R.B. and Pagano, N.J. (1970), "Interlaminar stresses in composite laminates under uniform axial extension", *J. Compos. Mater.*, **4**(4), 538-548.
Ramalingeswara, R. and Ganesan, N. (1996), "Interlaminar stresses in shells of revolution", *Mech. Comp. Mater. Struct.*, **3**(4), 321-329.
Ramalingeswara, R. and Ganesan, N. (1997), "Interlaminar stresses in spherical shell", *Comput. Mater. Struct.*, **65**(4), 575-583.
Reddy, J.N. (2003), *Mechanics of Laminated Composite Plates and Shells: Theory and Analysis*, CRC Press, New York.
Ren, J.G. (1987), "Exact solution for laminated cylindrical shell in cylindrical bending", *Compos. Sci. Tech.*, **29**(3), 168-187.
Sarvestani, H.Y. and Sarvestani M.Y. (2011), "Interlaminar stress analysis of general composite laminates", *Int. J. Mech. Sci.*, **53**(11), 958-967.
Shim, D.J. and Lagace, P. A. (2005), "An analytical method for interlaminar stresses due to global effects of ply drop-offs", *Mech. Adv. Mater. Struct.*, **12**(1), 21-32.
Tahani, M. and Nosier, A. (2003), "Free edge stress analysis of a general cross-ply composite laminates under extension and thermal loading", *Compos. Struct.*, **60**(1), 91-103.

Tang, S. and Levy, A. (1975), "A boundary layer theory-part II: extension of laminated finite strip", *J. Compos. Mater*., **9**(1), 42-52.
Tong, J.W., Xie, M.Y. and Shen, M., and Li, H.Q. (2001), "The Interlaminar Stresses of Symmetric Composite Laminates", *J. Reinf. Plast. Compos*., **20**(13), 1171-1182.
Varadan, T.K. and Bheskar, K. (1991), "Bending of laminated orthotropic cylindrical shells- an elasticity approach", *Compos. Struct*., **17**(2), 141-156.
Waltz, T.L. and Vinson, J.R. (1976), "Interlaminar stresses in laminated cylindrical shells of composite material", *AIAA J.*, **14**(76), 1213-1218.
Wang, A.S.D. and Crossman, F.W. (1977a), "Edge effects on thermally induced stresses in composite laminates", *J. Compos. Mater*., **11**(3), 300-312.
Wang, A.S.D. and Crossman F.W. (1977b), "Some new results on edge effect in symmetric composite laminates", *J. Compos. Mater*., **11**(1), 92-106.
Wang, S.S. and Choi, I. (1982a), "Boundary-layer effects in composite laminates. Part II: Free-edge stress solutions and basic characteristics", *ASME J. Appl. Mech*., **49**(3), 549-560.
Wang, S.S. and Choi, I. (1982b), "Boundary-layer effects in composite laminates. Part I: Free-edge stress singularities", *ASME J. Appl. Mech*., **49**(3), 541-548.
Wang, X. and Li, S.J. (1992), "Analytical solution for interlaminar stresses in a multilaminated cylindrical shell under thermal and mechanical loads", *Int. J. Solid. Struct*., **29**(10), 1293-1302.
Wang, X., Cai, W. and Yu, Z.Y. (2002), "An analytic method for interlaminar stress in a laminated cylindrical shell", *Mech. Adv. Mater. Struct*., **9**(2), 119-131.
Whitcomb, J.D., Raju, I.S. and Goree, J.G. (1982), "Reliability of the finite element method for calculating free edge stresses in composite laminates", *Comput. Struct*., **15**(1), 23-37.
Wu, H. and Yan, X. (2005), "Interlaminar stress modeling of composite laminates with finite element method", *J. Reinf. Plast. Compos*., **24**(3), 235-258.
Wu, Z. and Chen, W. (2010), "A global-local higher order theory including interlaminar stress continuity and C^0 plate bending element for cross-ply laminated composite plates", *Comput. Mech*., **45**(5), 387-400.

CC

Appendix A

In the LWT, the rigidity of thick shell can be obtained by carrying out the integrations in (12). Considering the Lagrangian interpolation function (5), the rigidity vectors $\tilde{A}_{pq}^{k}$ and B_{pq}^{k} are obtained as

$$(\tilde{A}_{pq}^{k},B_{pq}^{k})=\begin{cases}-\bar{C}_{pq}^{(1)}(\dfrac{r_2+r_1}{2R}), & t_1\dfrac{\bar{C}_{pq}^{(1)}}{2} & if\ k=1\\ \bar{C}_{pq}^{(k-1)}(\dfrac{r_k+r_{k-1}}{2R})-\bar{C}_{pq}^{(k)}(\dfrac{r_{k+1}+r_k}{2R}), & t_{k-1}\dfrac{\bar{C}_{pq}^{(k-1)}}{2}+t_k\dfrac{\bar{C}_{pq}^{(k)}}{2} & if\ 1<k<N+1\\ \bar{C}_{pq}^{(N)}(\dfrac{r_{N+1}+r_N}{2R}), & t_N\dfrac{\bar{C}_{pq}^{(N)}}{2} & if\ k=N+1\end{cases} \quad \text{(A-1)}$$

where in (A-1), $r_k=R+z_k$ is radius of k^{th} numerical surface. The rigidity matrix of the thick shell can be obtained by carrying out the integration in (12) as

$$(\tilde{A}_{pq}^{kj},B_{pq}^{kj})=\begin{cases}\dfrac{-\bar{C}_{pq}^{(k-1)}(r_{k-1}+r_k)}{2Rt_{k-1}}, & \dfrac{\bar{C}_{pq}^{(k-1)}}{2} & j=k-1\\ \dfrac{\bar{C}_{pq}^{(k-1)}(r_{k-1}+r_k)}{2Rt_{k-1}}+\dfrac{\bar{C}_{pq}^{(k)}(r_k+r_{k+1})}{2Rt_k}, & \dfrac{\bar{C}_{pq}^{(k-1)}}{2}-\dfrac{\bar{C}_{pq}^{(k)}}{2} & j=k\\ \dfrac{-\bar{C}_{pq}^{(k)}(r_k+r_{k+1})}{2Rt_k}, & t_{k-1}\dfrac{\bar{C}_{pq}^{(k)}}{6} & j=k+1\\ 0, & 0 & if\ j<k-1\ or\ j>k+1\end{cases} \quad \text{(A-2)}$$

and $\tilde{\tilde{D}}_{pq}^{kj}$ can be obtained as

$$\tilde{\tilde{D}}_{pq}^{kj}=\begin{cases}\dfrac{R\bar{C}_{pq}^{(k-1)}}{t_{k-1}}(\dfrac{r_k+r_{k-1}}{2}-\dfrac{r_kr_{k-1}}{t_{k-1}}\ln\dfrac{r_k}{r_{k-1}}) & j=k-1\\ \dfrac{R\bar{C}_{pq}^{(k-1)}}{t_{k-1}}(\dfrac{r_k-3r_{k-1}}{2}+\dfrac{r_{k-1}^2}{t_{k-1}}\ln\dfrac{r_k}{r_{k-1}})+\dfrac{R\bar{C}_{pq}^{(k)}}{t_k}(\dfrac{r_k-3r_{k+1}}{2}+\dfrac{r_{k+1}^2}{t_{k+1}}\ln\dfrac{r_{k+1}}{r_k}), & j=k\\ \dfrac{R\bar{C}_{pq}^{(k-1)}}{t_k}(\dfrac{r_{k+1}+r_k}{2}-\dfrac{r_{k+1}r_k}{t_k}\ln\dfrac{r_{k+1}}{r_k}) & j=k+1\\ 0 & if\ j<k-1 or\ j>k+1\end{cases} \quad \text{(A-3)}$$

and in (38)

$$(\tilde{\tilde{B}}_{pq}^{k})=\begin{cases} R(-\bar{C}_{pq}^{(1)}+\bar{C}_{pq}^{(1)}\dfrac{r_2}{t_1}\ln(\dfrac{r_2}{r_1})) & if\ k=1 \\ R(\bar{C}_{pq}^{(k-1)}-\bar{C}_{pq}^{(k)}+\bar{C}_{pq}^{(k-1)}\dfrac{r_{k-1}}{t_{k-1}}\ln(\dfrac{r_{k-1}}{r_k})+\bar{C}_{pq}^{(k)}\dfrac{r_{k+1}}{t_k}\ln(\dfrac{r_{k+1}}{r_k})) & if\ 1<k<N+1 \\ R(\bar{C}_{pq}^{(n-1)}+\bar{C}_{pq}^{(n-1)}\dfrac{r_{n-1}}{t_{n-1}}\ln(\dfrac{r_{n-1}}{r_n}) & if\ k=N+1 \end{cases} \quad \text{(A-4)}$$

Appendix B

The square matrices $[A]$ and the vector $\{F\}$ appearing in (19) are given as follows

$$[A]=\begin{bmatrix} [0] & [I] & [0] & [0] \\ [a_{21}] & [0] & [0] & [a_{24}] \\ [0] & [0] & [0] & [I] \\ [0] & [a_{42}] & [a_{43}] & [0] \end{bmatrix} \quad \text{(B-1)}$$

$$\{F\}=\{\{0\}^T,\{0\}^T,\{0\}^T,\{c\}^T\}^T \quad \text{(B-2)}$$

where the square matrices [0] and [I] are (N+1)×(N+1) zero and identity matrices, respectively and {0} is the zero vector with (N+1) rows and

$$[a_{21}]=[\tilde{\tilde{D}}_{22}]^{-1}([\tilde{\tilde{D}}_{44}]-R([B_{44}]+[B_{44}]^T)+R^2[\tilde{A}_{44}]+R^2[\alpha]) \quad \text{(B-3)}$$

$$[a_{24}]=[\tilde{\tilde{D}}_{22}]^{-1}(-[\tilde{\tilde{D}}_{22}]-[\tilde{\tilde{D}}_{44}]-R[B_{23}]+R[B_{44}]^T) \quad \text{(B-4)}$$

$$[a_{42}]=[\tilde{\tilde{D}}_{44}]^{-1}([\tilde{\tilde{D}}_{22}]+[\tilde{\tilde{D}}_{44}]+R[B_{23}]^T-R[B_{44}]) \quad \text{(B-5)}$$

$$[a_{43}]=[\tilde{\tilde{D}}_{44}]^{-1}([\tilde{\tilde{D}}_{22}]+R([B_{23}]+[B_{23}]^T)+R^2[\tilde{A}_{33}]+R^2[\alpha]) \quad \text{(B-6)}$$

$$\{c_1\}=[\tilde{\tilde{D}}_{44}]^{-1}(R^2\{\tilde{A}_{13}\}+R\{B_{12}\})\varepsilon_0 \quad \text{(B-7)}$$

It is to be noted that $[\alpha]$ is an (N+1)×(N+1) matrix whose elements are given by

$$\alpha^{kj}=\alpha\int_{-h/2}^{h/2}\Phi_k\Phi_j(1+z/R)dz \quad \text{(B-8)}$$

where α is a very small number compared to rigidities $\tilde{A}_{44}^{kj}-\frac{1}{R}B_{44}^{kj}-\frac{1}{R}B_{44}^{jk}+\frac{1}{R^2}\tilde{\tilde{D}}_{44}^{kj}$ and $\frac{1}{R^2}\tilde{\tilde{D}}_{22}^{kj}+\frac{1}{R}B_{23}^{kj}+\frac{1}{R}B_{23}^{jk}+\tilde{A}_{33}^{kj}$. The small artificial terms $\alpha^{kj}V_j$ and $\alpha^{kj}W_j$ are added to the right-hand side of (13), respectively, so that the eigenvalues in (23) will all be distinct (see (Ahmadi 2005) for more discussions on this subject).